REPUBLIC OF TURKEY
FIRAT UNIVERSITY
THE INSTITUTE OF NATURAL AND APPLIED SCIENCES
FACULTY OF SCIENCE

INVESTIGATION OF THE EFFECTS OF PRASEODYMIUM DOPING ON THE STRUCTURAL PROPERTIES OF HYDROXYAPATITE: AN EXPERIMENTAL AND THEORETICAL STUDY

Riyadh Saeed AGID

Master's Thesis

Department of Physics

JANUARY 2020

REPUBLIC OF TURKEY
FIRAT UNIVERSITY
THE INSTITUTE OF NATURAL AND APPLIED SCIENCES
FACULTY OF SCIENCE

Department of Physics

Master's Thesis

INVESTIGATION OF THE EFFECTS OF PRASEODYMIUM DOPING ON THE STRUCTURAL PROPERTIES OF HYDROXYAPATITE: AN EXPERIMENTAL AND THEORETICAL STUDY

Thesis Author

Riyadh Saeed AGID

Supervisor: Assoc. Prof. Dr. Ömer KAYĞILI

JANUARY 2020
ELAZIĞ

REPUBLIC OF TURKEY
FIRAT UNIVERSITY
GRADUATE SCHOOL OF NATURAL AND APPLIED SCIENCES

Physics Department
Atomic and Molecular Physics

Master's Thesis

Title: Investigation of The Effects of Praseodymium Doping on The Structural Properties of Hydroxyapatite: An Experimental and Theoretical Study

Author: Riyadh Saeed AGID

First Delivery: 04.12.2019

Date of Defense: 03.01.2020

THESIS APPROVAL

This thesis was prepared according to the rules of Firat University, Graduate School of Natural and Applied Sciences. It was evaluated by the jury members who have signed the following signatures and accepted unanimously because of the defense made available to the academic audiences.

		Signature	
Advisor:	Assoc. Prof. Dr. Ömer KAYĞILI Firat University, Faculty of Science		I Approved
Chairman:	Prof. Dr. Sinan AKPINAR Firat University, Faculty of Science		I Approved
Member:	Assoc. Prof. Dr. Bayram GÜNDÜZ Malatya Turgut Özal University, Faculty of Engineering		I Approved

This thesis was registered at the meeting of the board of directors of the institute on

/ / 20

Signature

Prof. Dr. Soner ÖZGEN

Director of the Institute

ACKNOWLEDGMENT

First of all, I would like to express my sincere gratitude to my supervisor: Assoc. Prof. Dr. Ömer KAYĞILI for his constant support of my thesis study and for his patience, motivation, and enormous knowledge. He is guidance helped me all the time from researching and writing this thesis. Thank you very much for your encouragement.

I would like to thanks also my Co-supervisor Prof. Dr. Niyazi Bulut for his constant help in part of the theoretical study of my thesis.

I would like to thank my family and friends: my mother, wife, daughter, brothers, and sisters for continuous supporting me. Finally, I would like to especially thank my wife. She was always there cheering me up and stood by me through the good times and bad.

This work was supported by the Management Unit of Scientific Research projects of Firat University (FÜBAP) (Project Number: FF.18.26).

Sincerely

Riyadh Saeed AGID

ELAZIĞ, 2020

TABLE OF CONTENTS

Page No.

ABSTRACT

Investigation of The Effects of Praseodymium Doping on The Structural Properties of Hydroxyapatite: An Experimental and Theoretical Study

Riyadh Saeed AGID

Master's Thesis

FIRAT UNIVERSITY
GRADUATE SCHOOL OF NATURAL AND APPLIED SCIENCES

Department of Physics
January 2020, Pages: ix +52

Calcium orthophosphates are a group of bioceramics that have been extensively used for medical purposes, especially for hard tissue engineering. More recently, the study and improvement in such bioceramics have made significant contributions to the health and quality of human life. Hydroxyapatite ($Ca_{10}(PO_4)_6(OH)_2$, HAp) is an important member of the calcium orthophosphate family and has high biocompatibility, osteoconductivity, and bioactivity. HAp can be used as an implant material for the damaged part of the human skeleton system because it has a similar chemical composition to natural human bones.

For this master thesis, five samples of hydroxyapatite (HAp) doped with praseodymium (Pr) at various amounts (2, 4, 6, 8 and 10 at.%) were synthesized by using the wet chemical route and characterized experimentally by using Fourier transform infrared (FTIR) spectroscopy, X-ray diffraction (XRD), energy dispersive X-ray (EDX) and scanning electron microscopy (SEM) techniques, cytotoxicity test, thermogravimetric and differential thermal analyses. Additionally, all samples were modeled by using the Quantum Espresso software and theoretically characterized by using the density functional theory (DFT).

The influence of Pr into the crystal lattice of HAp was observed. While a gradual increase in the crystallite sizes, lattice parameter *a* and unit cell volume was found, and a gradual decrease in the crystallinity degree was detected. Pr content from 2 to 10 at.% did not affect the thermal stability of HAp. The theoretical results showed that the bandgap energy of HAp decreased steadily from 3.82 eV to 1.32 eV with adding of Pr, and the density of states (DOS) was also affected by Pr content. The cell viability tests showed that among all the as-synthesized samples the best biocompatible properties were found for the sample, which is doped with 10 at.% Pr. Except for the sample having 6 at.% Pr, all the remaining samples were found to be potentially good candidates for biomedical applications.

Keywords: Hydroxyapatite; Praseodymium; Wet chemical method; X-ray diffraction (XRD); Band structure.

ÖZET

Praseodim Katkısının Hidroksiapatitin Yapısal Özellikleri Üzerine Etkisinin Araştırılması: Deneysel ve Teorik Çalışma

Riyadh Saeed AGID

Yüksek Lisans Tezi

FİRAT ÜNİVERSİTESİ
Fen Bilimleri Enstitüsü

Fizik Anabilim Dalı
Ocak 2020, Sayfa: ix +52

Kalsiyum ortofosfatlar, tıbbi amaçlar için, özellikle sert doku mühandisliği için, yaygın olarak kullanılan kullanılan bir grup biyoseramikleridir. Daha yakın bir zamanda, bu tür biyoseramiklerdeki çalışma ve gelişme, insan yaşamının sağlığı ve kalitesine önemli katkılarda bulunmuştur. Hidroksiapatit ($Ca_{10}(PO_4)_6(OH)_2$, HAp), kalsiyum fosfat ailesinin önemli bir ferdidir ve yüksek biyouyumluluğa, osteokondüktifliğe ve biyoaktifliğe sahiptir. HAp, doğal insan kemikleriyle kimyasal bileşim olarak benzerliği sebebiyle insan iskelet sisteminin zarar görmüş kısımlarının tedavisinde implant malzemesi olarak kullanılabilir.

Bu yüksek lisans tezi için, farklı miktarlarda (2, 4, 6, 8 and 10 at.%) praseodim (Pr) karkılı beş hidroksiapatit (HAp) numunesi yaş kimyasal yöntem kullanılarak sentezlendi ve Fourier dönüşümlü kızılötesi (FTIR) spektroskopisi, X-ışını kırınımı (XRD), enerji dağılımlı X-ışını (EDX) ve taramalı electron mikroskopisi (SEM) teknikleri, sitotoksisite testi, termogravimetrik ve diferansiyel termal analiz kullanılarak deneysel olarak karakterize edildi. İlave olarak, tüm numuneler Quantum Espresso yazılımı kullanılarak modellendi ve yoğunluk fonksiyonel teorisi (DFT) kullanılarak teorik olarak karakterize edildi.

Pr'un HAp'nin Kristal örgüsüne nüfuz ettiği gözlendi. Kristal büyüklüklerinde, örgü parametresi *a* ve birim hücre hacminde kademeli bir artış bulunurken ve kristalleşme derecesinde kademeli bir düşüş tespit edildi. %2 den %10'a (at.%) Pr içeriği HAp'in termal kararlılığını etkilemedi. Teorik sonuçlar Pr ilavesiyle bant aralığı enerjisinin 3.82 eV'tan 1.32 eV'a sürekli düştüğünü gösterdi ve durum yoğunlukları da Pr içeriğinden etkilendi. Hücre canlılığı testleri, tüm sentezlenen numuneler arasında en iyi biyouyumlu özelliklerin %10 (at.%) Pr ile katkılanan numune için bulunduğunu gösterdi. %6 (at.%) Pr'a sahip numune haricinde geri kalan tüm numunelerin biyomedikal uygulamalar için iyi birer potansiyel aday oldukları bulundu.

Anahtar Kelimeler: Hidroksiapatit; Praseodim; Yaş kimyasal yöntem; X-ışını kırınımı (XRD); Band yapısı.

LIST OF FIGURES

Page No.

LIST OF TABLES

Page No.

LIST OF ABBREVIATIONS

Symbol

HAp	: Hydroxyapatite
Pr	: Praseodymium
DFT	: Density functional theory
wt.%	: Weight percent
at.%	: Atomic percent
ACP	: Amorphous calcium phosphate
ε	: Tensile Strength
^{o}C	: Degree Celsius
$CaPO_4$	: Calcium orthophosphate
β-TCP	: Beta tricalcium phosphate
TetCP	: Tetracalcium phosphate
CMP	: Calcium metaphosphate
MCPM	: Monocalcium phosphate monohydrate
DCPD	: Dicalcium phosphate dihydrate
OCP	: Octacalcium phosphate
FAp	: Fluorapatite
hrs.	: Hours
XRD	: X-ray diffraction
FTIR	: Fourier transform infrared
SEM	: Scanning electron microscopy
EDX	: Energy dispersive X-ray
REE	: Rare earth elements
MTT	: Thiazolyl blue tetrazolium blue
M	: Molarity
DTA	: Differential thermal analysis

TGA	: Thermogravimetric analysis
FWHM	: Full width at half maximum
VB	: Valence band
CB	: Conduction band
HOMO	: Higher Occupied Molecular Orbital
LUMO	: Lower Unoccupied Molecular Orbital
eV	: Electron volt
E_g	: Energy gap

1. INTRODUCTION

Early civilizations have been named depending upon the stage of their material into three major historical periods; the first is the Stone Age, Bronze Age, and Iron Age, respectively. About two million years ago people start of the stone age began to make tools from stone which there used to arm himself against any threat to their existence, in that era, other natural materials have been used; wood, clay, and skins. Metals and minerals have been first identified in human history in the Bronze Age this period continued until the 9th century BC when man knew copper and the way bronze was made. Iron Age is the last age or era in the prehistory; the use of the iron element has been remarkably developed in this era, this age continued until the time of writing and the beginning of history [1].

In recent years ago, scientists have developed the sciences and technology to improve the quality of life and achieve prosperity for the present and future generations. Among these sciences are the study evaluation and understanding of the relationship between the structural chemical composition of the material and their properties. For the purpose of improving these properties to become more suitable for different applications and access to new materials with distinct characteristics suitable for the interdisciplinary fields of sciences, this development in technology is called material science.

A significant number of materials have been progressed; in the construction of medical devices and each of them has a special interaction with the material in some way with biological conditions, called these materials "biomaterials". In 1986, biomaterial was defined more accurately in the Consensus for Biomaterials of the Conference of the European Community, as “a non - viable material used to interact with biological systems in a medical device”. The areas of biomaterials are expanding in their ability to participate in many scientific disciplines [2].

The human body begins to grow up the age from the moment they are conceived. They face diseases or even a few injuries that could cause harm or loss of a part of the hard and soft tissues within the organic system. Bone and teeth diseases have become the most critical and life-threatening, where more than half a million people are diagnosed annually, and others die every year due to these diseases.

The skeletal system is an important structural component of the human body. Approximately half a million hip prostheses operations are done every year, and over two billion dollars have been spent for bone, teeth and other organ replacement and reconstruction operations worldwide [3].

For this purpose, researchers are moving towards the implant materials and have used these to repair and replace of hard tissues. Calcium orthophosphates are a group of bioceramics that have been extensively used for medical purposes, especially for hard tissue engineering. More recently, the study and improvement in such bioceramics have made significant contributions to the health and quality of

human life. It can be considered that hydroxyapatite (HAp) one of the extremely biomaterials was used in this field, has received extensive attention in medical applications, due to the fact that it is a huge proportion of the elementary structure of the teeth and bone minerals. HAp has the chemical formula of $Ca_{10}(PO_4)_6(OH)_2$ with a Ca/P stoichiometric ratio of 1.67. HAp seems to be the unique suitable material for hard tissue replacement operations and has good biocompatibility, osteoconductive ability with bioactivity properties that result in no rejection from the human body [4]. As such the use of hydroxyapatite in biomedical applications deserves special attention.

1.1. Objectives

The main objective of this work was an investigation of the following tasks:

1) Synthesize praseodymium-doped hydroxyapatite (Pr-HAp) by wet chemical method.
2) Determine the effects of the doping of the rare-earth element of praseodymium on the structural properties and surface chemistry of HAp.
3) Pr-HAp samples are model by using the Quantum Espresso software and theoretically characterize by using the density functional theory (DFT).
4) Observe the biological reaction to Pr-HAp *in vitro* biocompatibility properties using spectrophotometry.

1.2. Outline

The thesis is organized as follows:

Chapter 1 provides a brief introduction related to steps to improving material science.

Chapter 2 provides an introduction to the structure of hard tissue.

Chapter 3 presents some medical materials used for medical applications.

Chapter 4 provides brief information on the calcium phosphates, in particular, hydroxyapatite and its applications in medicine.

Chapter 5 is divided into sections. The experimental section of this research is the synthesis of the Pr-doped HAps and characterization technique applied to the samples.

Chapter 6 presents all the results and their discussions.

Chapter 7 presents conclusions and future work.

2. COMPOSITION AND PROPERTIES OF HARD TISSUES (BONE AND TEETH)

2.1. Composition and Structure of Bone

Bone is a remarkably important component of our body composed of organic and inorganic phases having complex microstructures, which play a key role in major function is provides internal support and protection for the vital organs of the body [3]. The bone which contains mainly of collagen, calcium phosphate, water, 20 wt.%, 69 wt.% 9 wt.% respectively, as well as other remaining organic constituents in small quantities, including proteins, lipids, and polysaccharides, and this is schematically shown in Figure 2.1 [5].

Collagen: this term can be regarded as the matrix is in the form of small microfibers [6]. The crystallized and/or amorphous forms of calcium phosphates give stiffness to the bone [3]. HAp in the form of needles or plates are deposited in parallel with collagen fibers so that the largest dimension of the crystals is along the long axis of the fibers [7]. Water plays a key role in the biomineralization process and enhancing mechanical properties.

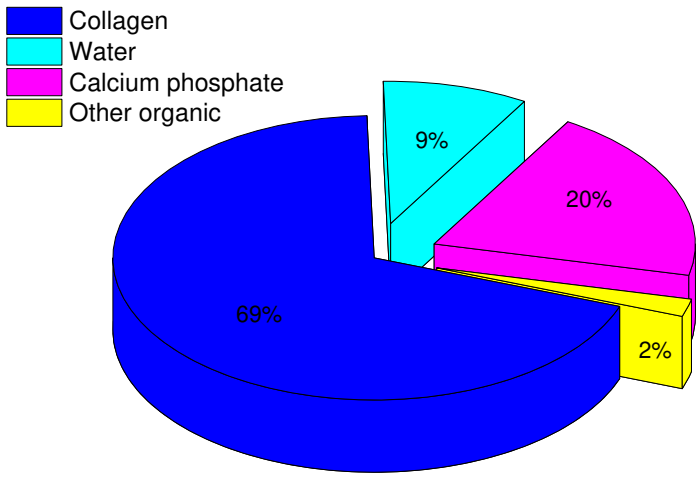

Figure 2.1. Pie charts of a typical human bone constituent by percent of the mass weight

Bone has been classified into two main types are compact bone and spongy bone [7]. Compact bone is supportive and protective of our tissues, which is hardest and denser compared to spongy bone.

Spongy bone is more active metabolically in comparison to the compact bone owing to the directional arrangement of collagen fibers and HAp crystals. Some mechanical properties of the human bones are summarized in Table 2.1.

Table 2.1. Mechanical properties of the human bones [8]

Bone	Compact	Spongy
Modulus of elasticity (GPa)	14 – 27	0.011 – 3.12
Tangential modulus of elasticity (GPa)	7 – 17	0.023 – 1.5
Radial modulus of elasticity (GPa)	7–16	0.024 – 1.5
Density (g/cm^3)	1.545–2.118	0.055 – 0.0744
Tensile strength (MPa)	150	0.11 – 11

2.2. Bone Cells

There are four different types of bone cells: osteoblasts and osteocytes cells, which are having main function work in resorption while two other osteoclasts and bone lining cells play a role in bone formation [9].

The main engaged of osteocytes is adjusting the protein and inorganic contents of the surrounding matrix by secreting substances that dissolve the matrix and repairing the damaged bone. The osteoblast is the second type of bone cells. These cells are responsible for producing a new bone matrix called the bone osteoid by synthesizing and releasing proteins and other organic components, a process called bone formation. The third type of bone cell is the osteoclast cell, which is responsible for the osteolysis process including the decomposition of matrices by acids and proteolytic enzymes. Osteogenic cells or bone lining cells are the last type of bone cells. The main function of osteogenic cells is responsible for the immediate release of Ca in the bone if Ca in the blood is too low.

2.3. Structure of Teeth

Crown and root are two main parts of the tooth shown in Figure 2.2. The root is covered by a layer of cementum attached to the bone by the periodontal membrane (a layer of fibrous connective tissue). The crown is divided into two main parts, enamel, and dentin. Which is covered with enamel and this is the part usually visible white color in the mouth. The enamel consists of the relatively large of the calcium phosphate, only with moderate wear and contains an enormous percentage of HAp crystals almost 97w/w % and the remaining part organic substances and water. The layer below the enamel is called the dentin, it constitutes of the mineralized tissue similar in composition to regular compact bone [3].

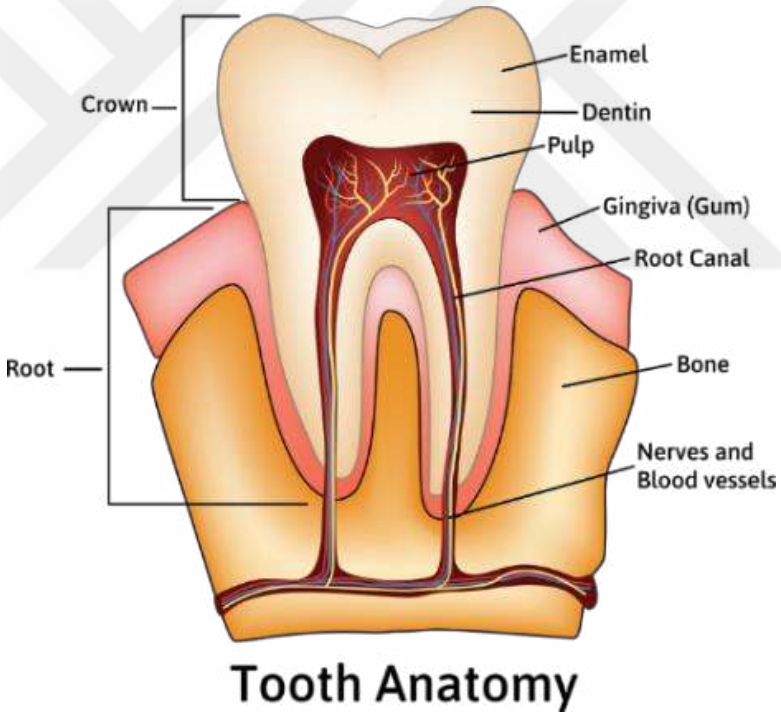

Figure 2.2. Tooth anatomy

The major elements present in the enamel, dentin, and bone, and their crystallographic parameters are tabulated in Table 2.2 [3].

Table 2.2. Chemical composition and crystallographic parameters of human bone and tooth [3]

Composition wt %	**Enamel**	**Dentin**	**Bone**
Ca^{2+}	36.5	35.1	34.8
P	17.7	16.9	15.2
Ca/P molar	1.63	1.61	1.71
Na^{+}	0.5	0.6	0.9
Mg^{2+}	0.44	1.23	0.72
K^{+}	0.08	0.05	0.03
CO_3^{2-}	3.5	5.6	7.4
F^{-}	0.01	0.06	0.03
Cl^{-}	0.3	0.01	0.13
$P_2O_7^{4-}$	0.022	0.1	0.07
Total inorganic (mineral)	97	70-65	65
Total organic	1.5	20	25
Absorbed H_2O	1.5	10	10
Lattice parameters			
a (nm)	0.9441	0.942	0.941
c (nm)	0.688	0.688	0.689
Crystallinity index	70-75	33-77	33-37
Ignition products (800 (°C)	β-TCP+ HAp	β-TCP+ HAp	HAp+CaO

3. BIOMEDICAL MATERIALS

Any substances either man-made or natural that is in direct contact with living cells or body fluids and the vital system in the human body are called biomedical materials, including joints and industrial metal plates to repair the fractures and must achieve full compatibility with the body clean [10]. Due to synthetic or natural materials contact with organs, tissues cells, proteins, and even organ systems, that including polymers, ceramics, inorganics, metals and natural macromolecules (biopolymers), which can be used for long-standing or temporary uses (e.g. artificial hip) (intravenous catheter) respectively. because of no single material is appropriate for repair and implement of bone and teeth, where at least more than one class of materials are combined together. Calcium phosphates are a group of biomaterial have been broadly used for the medical field, which it's a set of thirteen phases, start with tetra calcium phosphate (TetCP), and ending of the Calcium metaphosphate (α, β, γ) CMP, they have a molar ratio in the range from 0.5 to 2.0 respectively [11]. Even though the common uses of these materials in medicine, most of them do not provide all of the desired requirements to interact with body systems, thus, many of the current biomaterials have been improved to create new materials for the purpose of overcoming the problem [12].

Among these biomaterials, HAp is one of the most important biomaterials that has been widely used in medical applications since it represents a huge proportion of the elementary structure of the teeth and bone minerals, and its good biocompatibility profile and osseointegration ability. As such, the use of hydroxyapatite in biomedical applications deserves special attention. The next chapter deals with details information about the properties and characterization of the HAp and a brief summary of their synthesis.

3.1. Classification of Bioceramics

Bioceramics have been divided depending upon their field of application into three main generations, each with unique material has properties and applications in medicine, this dependence on interaction with the biological environment is most suitable with our body, those designed to interact with living tissues. (1) 1^{th} generation non-absorbable (2) 2^{nd} generation bioactive (3) 3^{rd} generation biodegradable [13].

3.1.1. First-Generation Non-Absorbable (Relatively Bioinert Bioceramics)

The so-called bioinert are biologically active and non-toxic materials meanwhile stimulates the interaction of a foreign body leading to a non-adherent fibrous capsule isolated from the surrounding bone. Because of this, studies efforts at the end of the past century had been devoted to biodegradable biochemistry [14].

Examples of bioinert bioceramics are alumina ($Al_2O_{3)}$, zirconium ($ZrO_{2)}$, titanium (Ti), stainless steel and high molecular weight polyethylene. Alumina and zirconia were the first ceramic materials to be used in orthopedic surgery. Between 1970 and 1990 this limited the uses of alumina and zirconia to femoral heads with a large and small diameter (32 mm), (28 mm) respectively. It is a material that does not appear in positive interaction with living tissue. As well as they do not undergo reactions with the medium in contact with physiological.

3.1.2. Second Generation Bioactive (Surface Reactive Ceramic)

Bioactive materials seem a positive interaction with body tissue that involves also the differentiation of immature cells to bone cells. Thus there will be biochemically-mediated strong bonding osteogenesis. Bioglasses and calcium phosphates are better bioactive materials used in the medical application. (e.g. bioglass) the increased phenomenon of adhesion, through stimulation of bone regrowth

3.1.3. Third Generation Biodegradable (Absorbable)

The resorbed material is replaced by endogenous tissue. Filling materials have enabling tissue deformation during and after their dissolution, which means that they actively contribute to the metabolic processes of an organism to reconstitute the tissue in part or in its entirety. Biodegradable chemically produced as the ceramic is resorbed must be able to be processed through the normal metabolic pathway of the body without evoking any deleterious effect. The main of bioresorbable materials are calcium phosphate compounds such as hydroxyapatite, tricalcium phosphate, calcium carbonate, and the biodegradable polyesters.

3.2. Material for Medical Application

3.2.1. Metallic Biomaterials

Metallic biomaterials have a superior mechanic property including resistance, strength, toughness, and fracture. Which is an essential class of material used in many medical applications especially that more used for load-bearing implants, such as hip and knee prostheses and also used as tools like pins, screws, and plates as shown in Figure 3.1. However, owing to there are a significant corrosive of some metals effects within the human body, would be used limited. Therefore, metals used in the body must have appropriate corrosion and wear resistance. Accordingly, alloys (metals containing two or more elements) are used for metallic implants. These three categories of metallic biomaterials are stainless steel, Co-Cr Mo, and Ti alloys [15].

Figure 3.1. Application of metallic biomaterials. Metals are used in medical devices such as plates, pins, orthodontists, rods and hip replacements

This can be used in any type of hard tissue in our body. Though the metallic biomaterials have unique mechanical properties, it has some disadvantages they easily get corroded in a few periods after their implantation in the host and It also has toxicity, these may influence the living organs where they

are repaired. Must take into account, when selecting metals and alloys depending on the surrounding condition of the host system.

3.2.2. Polymeric Biomaterials

Polymers are present as both synthetic or natural material, that made from groups of combined atoms together to form molecules of high molecular weight. Synthetic polymer materials including (polyethylene, polypropylene, poly (methyl methacrylate): PMMA.) as one of the best materials are widely used as medical materials as shown in Figure 3.2 because of their unique properties such as biodegradability, biocompatibility, lightweight, flexibility, reasonable cost, and non-corrosive, as well being ease of manufacturing to produce various shapes [16]. However, a limited group of polymers has been used for bone replacement purposes due to they not as strong as metals.

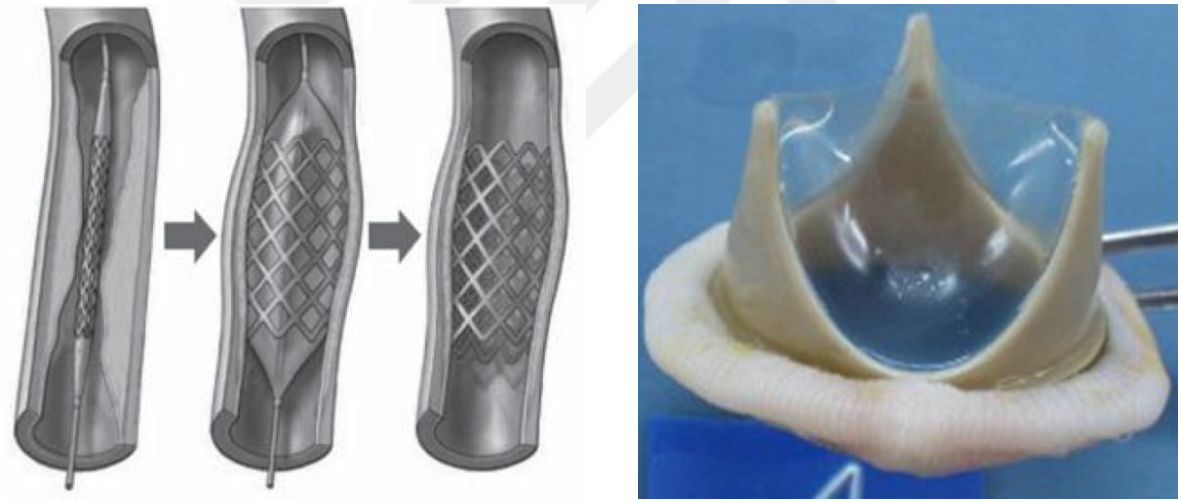

Figure 3.2. Applications of polymer biomaterials, (a) Balloon Angioplasty, (b) Polymer Heart Valves

3.2.3. Ceramic Biomaterials

Ceramic biomaterials are defined as synthetic materials that induce specific biological activity and function satisfactorily in a biological environment without damaging themselves or the environment. In addition, they are biocompatible materials, and generally include calcium phosphates and bioglass (which includes β-TCP and HAp), and biphasic calcium phosphate. However bioceramics were used to start with as an alternative biocompatible material to metallic bone implants, but because of their advanced overall performance; bioceramics have now turn out to be one of the most extensively studied biomaterial for bone medical applications [17].

Functions of Bioceramics by following

- They have a low friction coefficient for the lubrication of joint surfaces
- Can be placed on surfaces of cardiac valves that prevent blood coagulation
- They act as a stimulating material for bone growth.

3.2.4. Composite Biomaterials

Composite is composed of two (or more materials), that come from metal, ceramic and polymer, where at least one of them is solid, reaching the properties which cannot be provided by any of the components separately. The purpose of the constituent material is to obtain a substance of higher stiffness, strength, and toughness, meanwhile, higher resistance to creep, corrosion, wear or fatigue compared to conventional materials. In addition, with a suitable range of components, we can also get a set of specific properties (electrical, thermal, and optical). Unfortunately, combined materials its difficult workability and relatively expensive. A composite material is composed primarily of a matrix, i.e. a continuous phase, which is armored with a reinforcement (reinforcement is a secondary phase), which is usually the discontinuous phase. Composites have progressively increased, and today composite materials entered in different fields in our world. Therefore, there are many composite biomaterials have been made and tested for many medical applications.

3.3. Biocompatibility

The ability of a material function satisfactorily without any detrimental influence on the tissues surrounding it or any deterioration of the material itself. Biocompatibility was defined more accurately by Williams, 1999, as “The materials ability to perform with an appropriate host response in a specific application” [10].

There are considerations when selecting biomaterials depending on the direct contact, bonding or subject to reactions with cells and tissues within the body, biocompatibility properties are an essential requirement of the material, which implies that the biocompatibility total absence of interaction between material and cells implanted. Because no instruments within the body can be considered as truly incorporated if it is ignored. The material and tissue should interact in the maximum suitable to maximize the powerful incorporation of the material into the relevant problems and to make a certain balance. Three significant characteristics of the biocompatibility properties: (1) Biochemically compatible, non-toxic, non-irritative, non-allergenic, and non-carcinogenic. (2) Biomechanically

compatible with surrounding tissues. (3) There must be bio-adhesiveness between the material and the surrounding tissues.

4. CALCIUM ORTHOPHOSPHATES

Calcium orthophosphates are a group of bioceramics that have been broadly used for the medical field, especially for hard tissue engineering. In the 1980s, which they first used in clinical applications and first incorporated in dentistry and orthopedics [18]. As known as various types of Calcium orthophosphates materials are a set of thirteen phases, namely monocalcium phosphate monohydrate (MCPM, $Ca(H_2PO_4)_2H_2O$), dicalcium phosphate dehydrate (DCPD, $Ca(H_2PO_4)_2 \cdot H_2O$), octacalcium phosphate (OCP, $Ca_8(HPO_4)_2(PO_4)_4 \cdot 5H_2O$), α-tricalcium phosphate (α-TCP, α-$Ca_3(PO_4)_2$), β-tricalcium phosphate (β-TCP, β-$Ca_3(PO_4)_2$), HAp, $Ca_{10}(PO_4)_6(OH)_2$), and FAp, $Ca_{10}(PO_4)_6F_2$. These substances differ from each other in terms of molar ratio Ca: P. The Ca:P molar ratios for calcium orthophosphates are in the range of 0.5-2.0 [19]. This phase is a significant parameter that determines the solubility and acidity of calcium orthophosphates. A low Ca: P molar ratio corresponds to highly acidic and water-soluble calcium orthophosphates. Lately, study and improvement on such bioceramics have made significant contributions to the health and quality of human life. Although $CaPO_4$ compositions have been considered, HAp with a Ca:P molar ratio of 1.67 has been extensively investigated, because HAp contains a chemical composition and structure compared with those of natural bone mineral [20, 21].

4.1. Background of Hydroxyapatite

Hydroxyapatite (HAp) is one of the most essential components of bioceramics, this component represents a large percentage of the initial of the teeth and bone minerals, can be used in the human body to substitute for the damaged part of the human skeleton system including drug delivery, bone formation promoter, dental and bone cements, bone filler, root canal filler, and dental implants because it has an associated chemical structure to natural human bone. In addition, HAp particles have been recently studied by Ezhaveni et al, the results showed that HAp molecules prevent the growth of many types of cancer cells in the body [22].

The term "apatite" describes a set of compounds (not only calcium phosphates) with a general formula in form $M_{10}(XO_4)_6Z_2$, where M^{2+} represents cation XO_4^{3-} and Z^- are anions. Basing on the elements M, X and Z, HAp has the molecular chemical formula of $Ca_{10}(PO_4)_6(OH)_2$, where M, X, and Z are represented calcium (Ca^{2+}), phosphorus (P^{5+}), and hydroxyl radical (OH^-) respectively, therefore, which constituted of 39%, 18.5%, and 3.38% by weights of Ca, P and OH, respectively [23]. As known as with Ca:P stoichiometric ratio of 1.67 for ideal HAp which gives the highest stability [14, 24]. HAp appears to be the unique suitable material for the human hard tissue replacement operations and has

good bioactivity, biocompatibility, and osteoconductive properties that result in no rejection from the human body [25]. Furthermore, they can easily form direct chemical bonds with living tissues because its primary structure contains calcium (Ca) and phosphate (P) as same as the chemical composition of human bones [26]. Previous studies showed bioactivity and a high degree of biocompatibility of HAp.

The crystal structure of HAp is a single phase and hexagonal system unit cell where $a = b \neq c$, $\alpha = \beta = 90°$ and $\gamma = 60°$.The system belongs to spacing group P63/m and the approximate lattice parameters $a = b = 0.9418$ nm and $c = 0.6884$ nm [23]. Additionally, HAp in general constitutes of Ca^{2+}, PO_4^{3-} and OH^- groups packed in a certain orientation as shown in Figure 4.1. Furthermore, HAp is similar in lattice parameter to the mineral component of bone a-axis and c-axis (nm) 0.9410 and 0.6890, respectively, some mechanical and chemical properties of the mineral phase of bone compared with synthesis HAp are summarized in Table 4.1 [27].

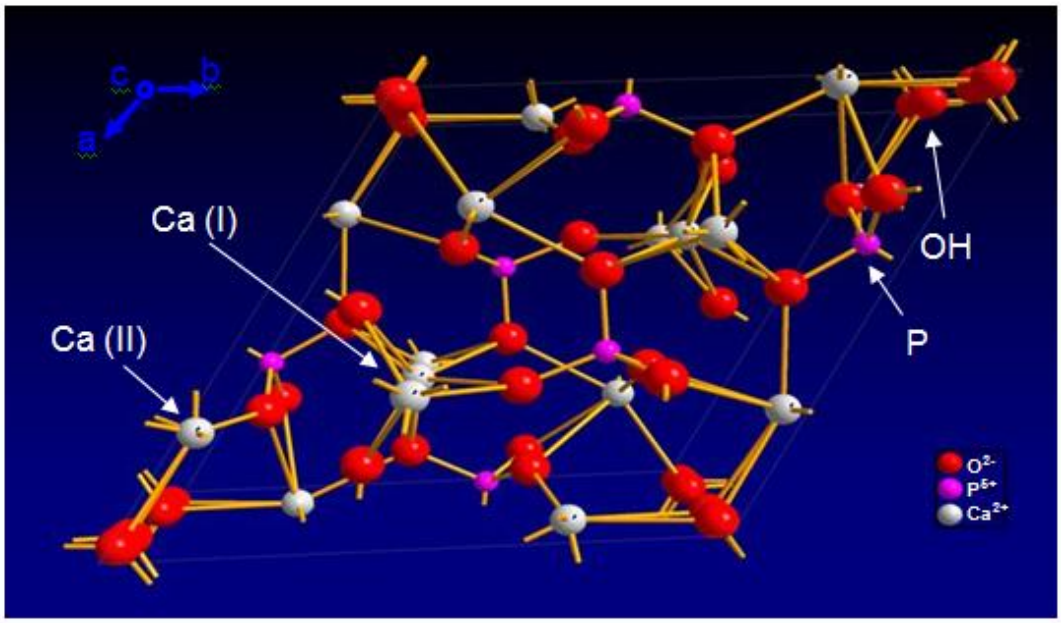

Figure 4.1. The molecular of hydroxyapatite $Ca_{10}(PO_4)_6(OH)_2$ [23]

There are two sites for calcium of HAp unit cell are Ca (I) and Ca (II), the first sit Ca (I) the position of four calcium atoms per unit cell within the parallel column to the c- axis is surrounded nine oxygen atoms as shown in Figure 4.1 [23]. The other site Ca (II) contains six calcium atoms per unit cell are position is called anion channel.

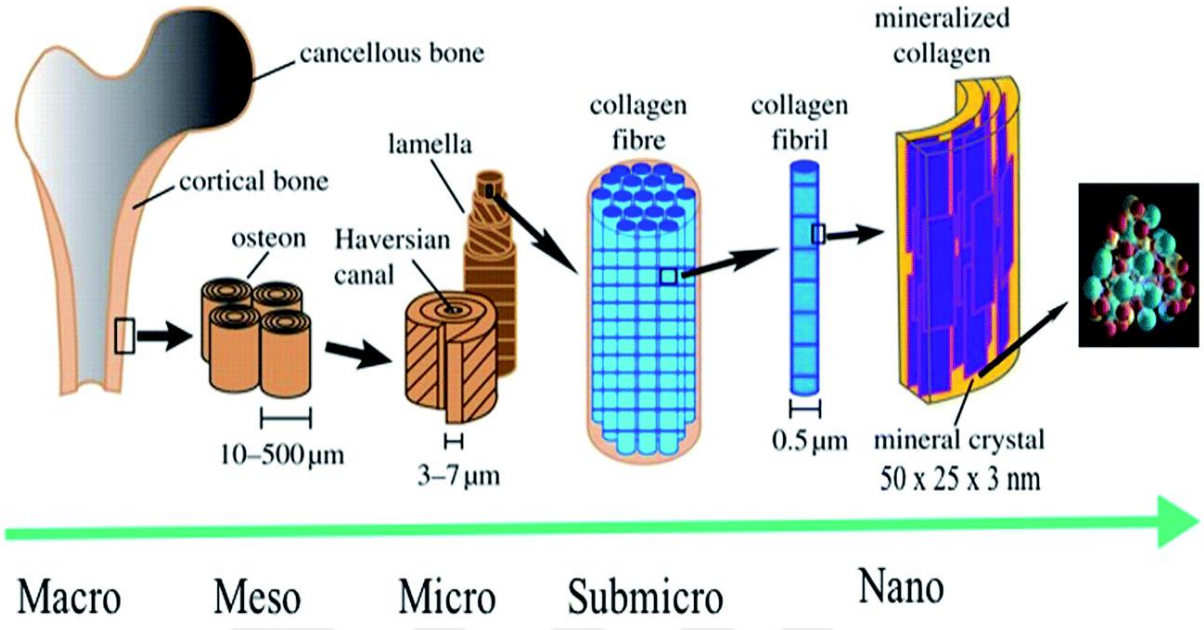

Figure 4.2. Schematic of the sophisticated hierarchical structure of bone

Many natural sources for HAp include, among others, human bone, bovine bone, coral, chitosan, fishbone, and eggshell. However, the transmission of diseases when proper preparation is not followed is a concern with natural HAp ignore all protein. Synthetic HAp is more commonly used because it is easier to access and free from the transmission of diseases. HAp exists in the bone as nanocrystals with dimensions of 50 x 25 x 3 nm as illustrated in Figure 4.2, in which nanocrystals are embedded in an organic collagen fiber matrix of 90 percent of the protein content [28].

4.1.1. Synthesis of HAp

Several techniques have been successfully employed for preparing pure HAp powders. Wet methods and dry methods are the two main ways of preparing HAp powders. For the wet chemical methods, aqueous solutions of Ca and P ions can be achieved by the number of technical methods, including precipitation, hydrolysis method, sol-gel method, hydrothermal method, emulsion method, and sonochemical method. Dry methods can be performed in two main ways: solid-state reactions and mechanochemical process. Dry methods, which are Classical methods have the convenience of producing highly crystalline HAp from relatively inexpensive raw materials. The main disadvantage either the large size of particles in the case of solid-state synthesis and the low phase purity of HAp in the case of the mechanochemical process. In recent years, progress in preparing HAp using dry

methods, especially solid-state method, has been very slow according to the literature about synthesizing HAp [29].

As previously mentioned the stoichiometric molar ratio is extensive important, it is necessary to take into account and while synthesis HAp, the nearer the value of Ca:P to 1.67, implies that the material inside the human body is more stable. In contrast, if that value of Ca:P decreases, it means that, better bioactivity. Another aspect that is important has been observed is the degree of crystallinity. It has been showed that the crystallinity in the tissues for the tooth is very high, while in the bone, it is very poor. This implies that the reactivity depends on the degree of crystallinity since the reactivity in bone is higher than in the tooth. This is required to consider, besides the above, that differences in the physical and chemical properties of apatites stand on the type of method and temperature in which are made [23]

4.1.2. Wet Chemical Method

In the present study, the wet chemical method is used for making hydroxyapatite. These methods are much quicker than conventional methods, due to their high surface area, simplicity, ready availability, relatively easy to drive and use low-cost raw materials, consider its one of the greatest common methods is wet chemical precipitation route. Wet methods have the most abundant been applied to the preparation of HAp components having a nanosized structure with regular morphology [29].

İnce et al [30] have synthesized Ni/Mg co-doped HAps by the wet chemical route and characterized their structural properties. They have demonstrated that it is easy to synthesize co-doping nanocrystalline HAp from raw materials by the wet chemical method. besides, and they also reported that there was a dramatically decreased crystallite size, lattice parameters, and crystallinity with the addition of Ni. There was observed change from the HAp phase to the β-TCP phase. these changes consequent to the difference between the ionic radius of Mg and Ca (0.065 nm), (0.099 nm), respectively, thus phase transition of HAp to β-TCP.

Table 4.1. Chemical and physical properties of the bone compared with synthesis HAp

Constituents (wt %)	**Bone**	**HAp**
Ca^{2+}	34.8-36.6	39.6
P	15.2-17.1	18.5
CO_3^{2+}	4.8-7.4	-
Na^{+}	0.7	-
K^{+}	0.03	-
Mg^{2+}	0.55	-
CO_3^{2+}		-
F^{-}	0.02	-
Cl^{-}	0.1	-
(Ca:P) molar	1.65	1.67
Mechanical properties		
Compressive strength MPa	100-230	120-900
Tensile strength MPa	50-150	38-300
Fracture toughness $MPa.m^{1/2}$	2-12	1
Young's elastic modulus GPa*	18-22	35-120
Hardness GPa	-	3-7

4.1.3. Substitutions of HAp

Manufactured hydroxyapatite is to some degree diverse in the concoction and physical properties to that hard tissue minerals. Although, pure HAp having well-documented biocompatibility and bioactivity. Unfortunately, the application of hydroxyapatite has been limited in medicine for hip joint replacement because of its poor physical properties such as brittleness and lack of strength. To overcome this problem, HAp has been doped or substituted with various elements.

An interesting aspect of hydroxyapatite structural characteristics is the ability to share ions the variety of substitutes in the structure such as cations and anions (or meanwhile both of them) without

changing their geometry. Bone mineral is typically Ca-deficient and contains carbonate substitutions. Other ions present in the bone mineral are Mg^{2+}, Na^{+}, K^{+}, F^{-}, and Cl^{-}. The more suitable general formula for HAp is (Ca, $M)_{10}(PO_4, Y)_6(OH, X)_2$ where *M* symbolizes a cation and *X* and *Y* symbolize anions [31].

The substitutions may cause changes in properties including solubility, especially biological response, and crystallinity. The researchers have tried to enhance the biological response of HAp through substitution. To improving the properties of HAp by substitution anion or cation into three stages as follows:

4.1.4. Anionic Substitution

Anionic substitution of hydroxyl groups (OH^{-}) with other monovalent anions with a charge balance, such as F^{-} or Cl^{-}, produces Trivalent anions (for example, PO_4^{3-} phosphate group) that can replace divalent anions but this exchange It is because of the formation of vacancies in the structure of HAp. The trivalent silicate (SiO_4^{-4}) can also be added to the HAp structure, in hydroxide vacancies. Results illustrated in Table 4.2 displays that the anions dopant of hydroxyl groups (OH^{-}), phosphate group (PO_4^{3-}) may affect the crystal structure of HAp.

Tetravalent silicate ($SiO4^{4-}$) substituted into the HAp (Si-HAp) by replacement of the trivalent anions phosphate group ($PO4^{3-}$). According to suggested some reports in which Si is necessary for the metabolic processes related to the growth and skeletal development and integrity of the extracellular matrix. Si is doped into HAp (Si-HAp), was synthesized via several technique methods, including that solid-state reaction [32], hydrothermal methods, precipitation methods [34], and sol-gel methods [35].

Aminian et al in 2011 by a hydrothermal technique has been successfully prepared Si-HAp, in this work, silicon was incorporated into hydroxyapatite (HAp) lattice through partially substituting PO_4^{3-} groups with SiO_4^4 ones resulting in Si-HAp. They found that the Si-HAp resulted in a reduction in the size of Si-HAp crystallites. Authors have found that this incorporation Si into HAp led to a significant reduction in the size of Si-HAp crystallites (however, the result showed that Si substitution does not influence the thermal stability of Si-HAp) [33].

Table 4.2. The impact of some anions substitutes to hydroxyl and phosphate group on the crystal structure of hydroxyapatite

Anions substitute	Ionic radius (nm)	Lattice parameter *a=b* (nm)	Lattice parameters *c* (nm)	Crystallinity
Pure HAp		0.9438	0.6822	
PO_4^{3-}				
CO_3^{2-}		(↓)	(↑)	(↓)
HPO_4^{2-}		(↑)	(nc)	(nc)
OH^-				
Cl^-	0.181	(↑)	(↓)	(nc)
F^-	0.136	(↓)	(nc)	(↑)

(↑) increase, (↓) decrease, and (nc) not change.

There are other researches have been shown that the incorporation of anions into a synthetic HAp structure such as carbonates substitutions instead of the trivalent phosphate group PO_4^{3-} [36], fluorine substituted hydroxyl groups OH^- [37], sulfur and selenium oxyanions [38].

4.1.5. Cationic Substitution

There are many studies conducted on the substitution of cations is much more than on the anions. Because the cation substitute properties of HAp are highly important for both waste management and catalysis applications. Most cations which can be extremely substituted into HAp include Mg, Zn, Sr, La, Cd, Pb, Cu and Fe [39], Table 4.3 summarizes the results of systematic revealing methods illustrated, the cation dopant of ions into the HAp structure will affect in some their crystal structural include morphology, lattice parameters, stability, and mechanical properties. The properties of synthesized hydroxyapatite differ depends on the properties of the ion substituting into the structure (ionic radius and charge, however, access to different electron orbits may be important) [40].

For example, the magnesium (Mg^{2+}) is among the most abundant substitution in hydroxyapatite. Mg, which is considered as the main important found element in the formation of bone and teeth after

Ca, K, and Na. The range of Mg concentrations in the natural dentin and bone is 1.23 wt% and 0.73 wt%, respectively. Precipitation method was mostly carried out to prepare Mg-HAp. Kaygili et al. [41] prepared magnesium substituted hydroxyapatite (Mg-HAp) via the combustion method at low temperature with different amounts of Mg (e.g., 1.2 at. % and 2.4 at. %). This study found that magnesium incorporated into the HAp resulted in a noticeable decrease in crystallite size, crystallinity, and *a, b* lattice parameter, but *c* parameter increased, owing to the considerably smaller radius of Mg^{2+} (0.069 nm) than of Ca.

Table 4.3. The impact of some cations replacements to Ca^{2+} on the crystal structure of hydroxyapatite

Cations substitute	**Ionic radius (nm)**	**Lattice parameter *a=b* (nm)**	**Lattice parameters *c* (nm)**	**Crystallinity**
Ca^{2+}	0.099	0.9438	0.6822	
Mg^{+}	0.066	$(\downarrow)^{++}$	$(\downarrow)^{++}$	$(\downarrow)^{++}$
Zn^{2+}	0.074	$(\uparrow)^{++}$	$(\uparrow)^{++}$	$(\uparrow)^{++}$
Al^{3+}	0.051	$(\uparrow)$	$(\uparrow)$	$(\downarrow)$
K^{+}	0.133	(nc)	(nc)	(nc)
Sr^{2+}	0.112	$(\uparrow)$	$(\uparrow)$	(nc)
Ba^{2+}	0.134	$(\uparrow)$	$(\uparrow)$	$(\downarrow)$
Pb^{2+}	0.120	$(\uparrow)$	$(\uparrow)$	$(\downarrow)$
Na^{+}	0.097	(nc)	(nc)	(nc)
Li^{+}	0.068	(nc)	(nc)	(nc)
Cd^{2+}	0.097	$(\downarrow)$	$(\downarrow)$	$(\downarrow)$
Mn^{2+}	0.080	$(\downarrow)$	$(\downarrow)$	$(\downarrow)$

$(\uparrow)$ increase, $(\downarrow)$ decrease, (nc) not change, $^{++}$ TCP second phase addition to HAp.

Ren et al. [42] carried out a computational study based on approximation density functional theory (DFT) using ab initio simulation to determine the changes in the lattice parameters and found that the trend of the results illustrates that the lattice parameter (*a* and *b*) decreased slightly with increased Mg concentration. These conflicts can be interpreted by the strong dependence of the lattice parameters on the preparation method [43].

Zn incorporated hydroxyapatite (Zn-HAp) has been abundantly studied, due to the key effect of Zn ions in several metabolic processes that make zinc eligible for use in many biomedical applications. Most of the work in research has been focused on the synthesis of zinc doped hydroxyapatite (Zn-HAp) using a precipitation method [44, 45]. Miyaji et al.[46] reported that the substitution limit for Zn is ~15 mol%.

4.1.6. Multi-Ionic Substitution(Co-Doping)

Several studies have explored the multiple ionic replacements that many researchers have succeeded in replacing in the HAp structure. There are three possible subcategories of multiple ionic replacements based on the type of HAp synthesized: cationic, anionic, and together cationic and anionic substitution.

These are affected by a variety of factors, such as crystal structure, lattice parameter, crystallinity, crystallite size and thermal stability these aspects of physical properties, Another aspect that is important has been observed is biological properties changed as well [24]. Yttrium and fluoride co-substituted hydroxyapatite structure, the mixtures were synthesized using precipitation method by Basar et al (2010) [47]. Observation from the results of this experiment seems to indicate the effect of the additives yttrium and fluoride to the pure HAp on the crystal structure (this has led to a decrease in lattice parameters and unit cell volumes).

In the case of anionic co-doped; fluoride/carbonate has been successfully doped into pure HAp by the wet chemical method, Sakae et al [48].

4.1.7. Lanthanide-Doped into Hydroxyapatite

A recent systematic review investigated some rare earth elements or lanthanides such as Gd^{3+}, La^{3+}, $Nd^{3+}$and $Ce^{3+}$are added to HAp to enhancement its biological properties and the promotion of bone remodeling [49]. Rare earth elements are a family of 17 metals, start from lanthanum and end with lutetium, there are generally two groups of lanthanides (i.e. light and heavy) [50]. Those have received attention because of their unique optical, magnetic and catalytic characteristics, lanthanide compounds can be used in different nanomedical fields, including treatment, imaging, and diagnosis [51]. HAp syntheses doped with lanthanide exhibited enhanced biological characteristics such as biocompatibility, cell adhesion, and proliferation compared to non-doped composites [52].

Praseodymium (Pr) is the third element in the lanthanide complexes group, considered to be a light-group of rare earth (LREE) with atomic number 59 [53]. Praseodymium is a soft, elastic rare-

earth element and silvery color. Besides, it occurs naturally or extracts with other rare earth in monazite and it has in oxidation number trivalent (III) rare-earth ion. It is very reactive and while systematized, it slowly progresses a green oxide coating. It reacts quite quick with warm water as compared slowly reacts with cold water and to obtain praseodymium hydroxide, and also reacts with oxygen inside the air to obtain praseodymium oxide. It further withstands to corrosion in the air than other lanthanide ions [54].

Due to some unique features make the praseodymium applicable to different fields such as industry and medicine. As mentioned above, Pr(III) occurs mixture naturally which forms as florid the center of carbon arc that can be used in creating animation pictures for studio lighting. Additional dopant silicate crystals were used with praseodymium ions to slow the light pulse to some hundred meters per second.

The biological properties of praseodymium ion and other lanthanide ions have an ionic radius of similarity value to Ca^{2+} ion [55]. These similarities are not constrained to their ionic radii but consist of an aspect in their coordinate range and binding behavior. further, that has a better charge, they have an excessive affinity for Ca^{2+} sites on biological molecules, and a stronger binding to water molecules [56]. Recently conducted studies indicate that lanthanide elements are found that in the human body including that liver, spleen, lung, and bone [57].

Osteoporosis is known to be the most common bone disease caused mainly by lack of Ca and minerals density, and therefore bones become more brittle and then increase the risk of fracture, other aspects contribute to structural disorders, including decreased physical activity, excessive drug and alcohol abuse, and cigarette addiction [49].

Calcium is the most interesting one inorganic biomaterial constituting about 36.5%, 35.1% and 34.8% of enamel, dentin, and bone, respectively because of its impact on cellular metabolism [58]. Treatment of osteoporosis disease is extensive difficult and depends upon many of the causes, such as age, the advancement of the disease, in order to increase bone mass and strength by inhibiting bone absorption, here are many drug treatments that can be applied [59].

To the best of our knowledge, present scientific reports show that some rare earth compounds such as complexes, nanoparticles, and many others can be successfully employed in the treatment of bone disorders as shown in Figure 4.3. Moreover, lanthanide-doped into hydroxyapatite making this as creating new material for multifunctional biomedical applications. The incorporation of lanthanide has an essential influence on the crystal structure, surface area, solubility, and thermal stability relative to without doped material.

Similar ionic radii of lanthanide ions are able to replace calcium in the hydroxyapatite component because rare earth metal ions may affect cell proliferation and differentiation [60]. It is worth mentioning that HAp nanoparticles structural is able to host materials can be functionalized using various types of dopants and substrates.

Interestingly, there are only a few studies concerning the rare earth elements doped hydroxyapatite. HAp replaced by lanthanide ions have been a focus of attention researchers for more than a decade, who have developed a bone-related biomaterial [61]. Yasukawa et al. [62] show that the improvement in the biological performance of lanthanide is solely as a result of their specific ability to replace Ca^{2+} in structured molecules. The recent studies indicated that lanthanum has an effect on the bone reshaping cycle and the ability to suppression or even the face of the impact of osteoporosis [63]. Serret et al [64] depend on the data obtained from the XRD, showed that the substitute of La^{3+} into the hydroxyapatite stabilized the apatite phase and the lack of significant changes in the crystal structure and the lattice parameters *a* and *c*. They also demonstrated that cation La^{3+} compact molecules of homogeneous solid solutions can form only in a limited time using strict Ln/ (Ln + Ca) atomic ratios. The study conducted by [62] also exhibited that regardless of the kind of lanthanide, both lattice parameters *a* and *c* go increased with the ratio of the increasing atoms from 0 to 0.05 due to substituting smaller Ca^{2+} ions by larger lanthanide cations.

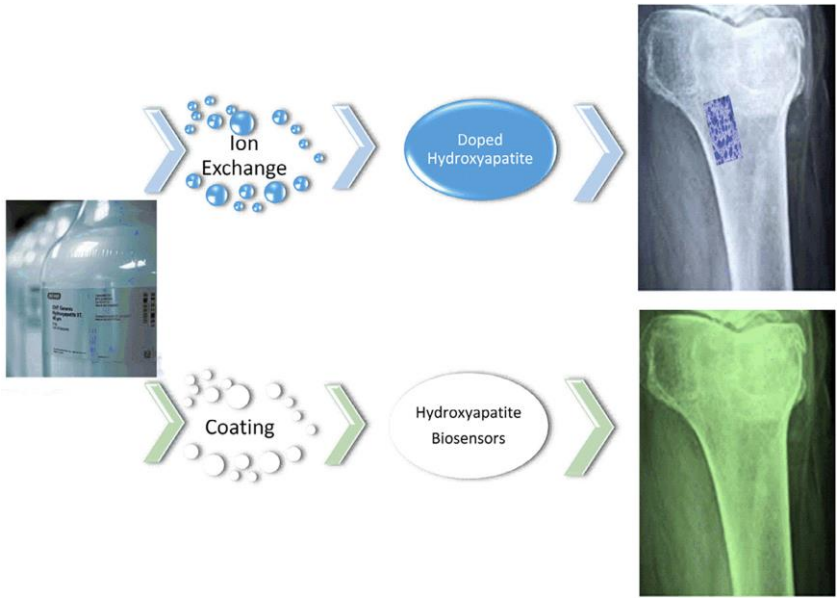

Figure 4.3. Hydroxyapatite modification improving its applicability in bone tissue engineering

5. EXPERIMENTAL PROCESSES

This chapter deals with the study of the synthesize and praseodymium doped on the HAp and brief information of the theory of the various examination instruments carried out in this study to characterize specimens. The X-ray diffraction (XRD) analysis was used for studying the crystal structure properties. Besides, scanning electron microscopy (SEM), and Fourier transforms infrared (FTIR) spectroscopy were used in order to study morphology and bonds of the samples, respectively. Biocompatibility and toxicity tests were screened in vitro for the synthesized Pr-HAp, the cytotoxicity values effects were determined by an indirect method with MTT (thiazolyl blue tetrazolium blue) test using spectrophotometry.

5.1. Materials

In this study, all main precursors required to the synthesis of Pr-HAp were purchased including those of calcium nitrate tetrahydrate ($Ca(NO_3)_2 \cdot 4H_2O$, Carlo-Erba), praseodymium (III) nitrate hexahydrate ($Pr(NO_3)_3 \cdot 6H_2O$, Alfa – Aesar) and di-ammonium hydrogen phosphate ($(NH_4)_2HPO_4$, Merck, Germany). Ammonium hydroxide (NH_4OH, Sigma, Aldrich) was used to maintain the pH value of Pr-doped samples.

5.2. Synthesis

Praseodymium (Pr)-doped hydroxyapatite was synthesized by using a wet chemical method. Pr was added in five different amounts and distilled water was used as the solvent. A 100 mL of (0.5-*x*) M $Ca(NO_3)_2 \cdot 4H_2O$ and *x* M $Pr(NO_3)_3 \cdot 6H_2O$ were dissolved in the distilled water in a beaker. Here, x represents praseodymium concentration (0.005, 0.010, 0.015, 0.020, and 0.025). 100 mL of 0.3 M $(NH_4)_2HPO_4$ solution was prepared in the different beaker, then poured drop by drop into $Ca(NO_3)_2 \cdot 4H_2O$ and $Pr(NO_3)_3 \cdot 6H_2O$ solution, and a milky white solution was obtained. For all the aqueous solutions, the pH was adjusted to a value of 10 by adding dropwise an aqueous solution of NH_4OH. At the end of the pH adjusting process, the mixture was stirred with a magnetic stir bar at room temperature aged for 2 hrs. and the gel formation was observed within this period. After that, this gel was dried in an oven at 130 ºC for 25 hrs. The as-dried samples were heated in an electric furnace at 870 ºC was left for 3hrs. and finally, Pr-doped HAp samples were obtained in the powder form. Depending on Pr amount, the prepared samples were named as 2 at.% Pr-HAp, 4 at.% Pr-HAp, 6 at.% Pr-HAp, 8 at.% Pr-HAp and 10 at.% Pr-HAp.

5.3. Characterization

5.3.1. XRD Investigations

X-ray diffraction investigations have been used for the identification of structural properties and phases of crystalline materials. To determination of crystallite size, crystallinity, and lattice constants in a specimen of amorphous and crystalline materials. A Rigaku RadB-DMAX II device was used. The samples were exposed to Cu-Kα radiation having a wavelength of 0.15406 nm.

5.3.2. FT-IR Analyses

Fourier transform infrared (FTIR) analyses were used to determine the functional group of all samples, within the scanning range from 400 to 4000 cm^{-1} was achieved using a PerkinElmer Spectrum One spectrometer, using KBr pellets.

5.3.3. SEM and EDX Analyses

A scanning electron microscope (SEM) is a type of microscope which employs an electron beam to produce an image of the sample. Its (SEM, FEI Quanta 450 FEG) equipped with an energy dispersive X-ray (EDX, Amatek Octane Plus) operated at 20 kV was used for studying morphology and determining the elemental compositions of the as-investigated sample.

5.3.4. DTA and TGA Analyses

For differential thermal (DTA) and thermogravimetric (TGA) analyses of dried powders were performed using Shimadzu DTA 50 and Shimadzu TGA 50, respectively. Both methods are useful to determine the effects of doping on the thermal stability and mass change of HAp as a function of increasing temperature. The thermal properties of the as-produced samples were studied in the range from 25 to 1000 °C.

5.3.5. The Investigation of *in Vitro* Biocompatibility Properties

The cytotoxicity values for 2 at.% Pr-HAp, 4 at.% Pr-HAp, 6 at.% Pr-HAp, 8 at.% Pr-HAp, and 10 at.% Pr-HAp samples were determined by an indirect method with MTT (thiazolyl blue tetrazolium blue) test using spectrophotometry. The experimental protocol was prepared according to ISO-10993-5 “Biological Evaluation of Medical Devices” standards. The mouse (Mus musculus) fibroblast cells (L-929) were used in this study. Firstly, samples were washed once with 70% ethanol and three times

with sterile PBS (pH 7.4). Then, samples were incubated in Dulbecco's Modified Eagle Medium (DMEM) using an incubator containing 5% of CO_2 at 37 °C for 72 hours. For the experiment, the L-929 cell line was grown at 37 °C containing 5% of CO_2 in DMEM medium. After reaching 80% confluence of the cells, they were removed from the flasks with 0.25% trypsin-EDTA solution. Then, followed by the centrifugation of the cells at 2000 rpm for 5 minutes and they were seeded into 96-well plates as 10^4 cells/well and incubated for 24 hours under the same conditions. At the end of the incubation period, another incubation time for 24 hours was applied for the samples by being exchanged DMEM medium with the medium in which samples were held for 3 days. Subsequently, 90 µL of fresh DMEM medium was added into the plates by removing the medium through the cells. Subsequently, 10 µL from 5 mg/mL MTT solution prepared with sterile PBS was added to the cells and incubated in dark for 4 hours under the same conditions. Then, the absorbance values of the purple color at 550 nm were measured using the ELISA microplate reader. The medium held for 72 hours in the incubator was added into wells for the control groups incubated under the same conditions and the cells in these wells were considered as 100% live. As a result, the cell viability of the samples on L-929 cells compared to the control groups was calculated.

6. RESULTS AND DISCUSSION

6.1. XRD Analysis

The XRD profiles of Pr-doped (2,4,6,8 and 10 at.%) were depicted in Figure 6.1 and the as-observed data were compared to the Joint Committee on Powder Diffraction Standards (JCPDS). As shown in Figure 6.1, all XRD patterns of Pr-HAp powders were matched with that of pure HAp (JCPDS PDF no. 09-0432). The broadness of the XRD peaks indicated to a low crystallinity of all Pr-doped HAps and no peaks related to other calcium-containing and/or Pr-containing compounds were detected.

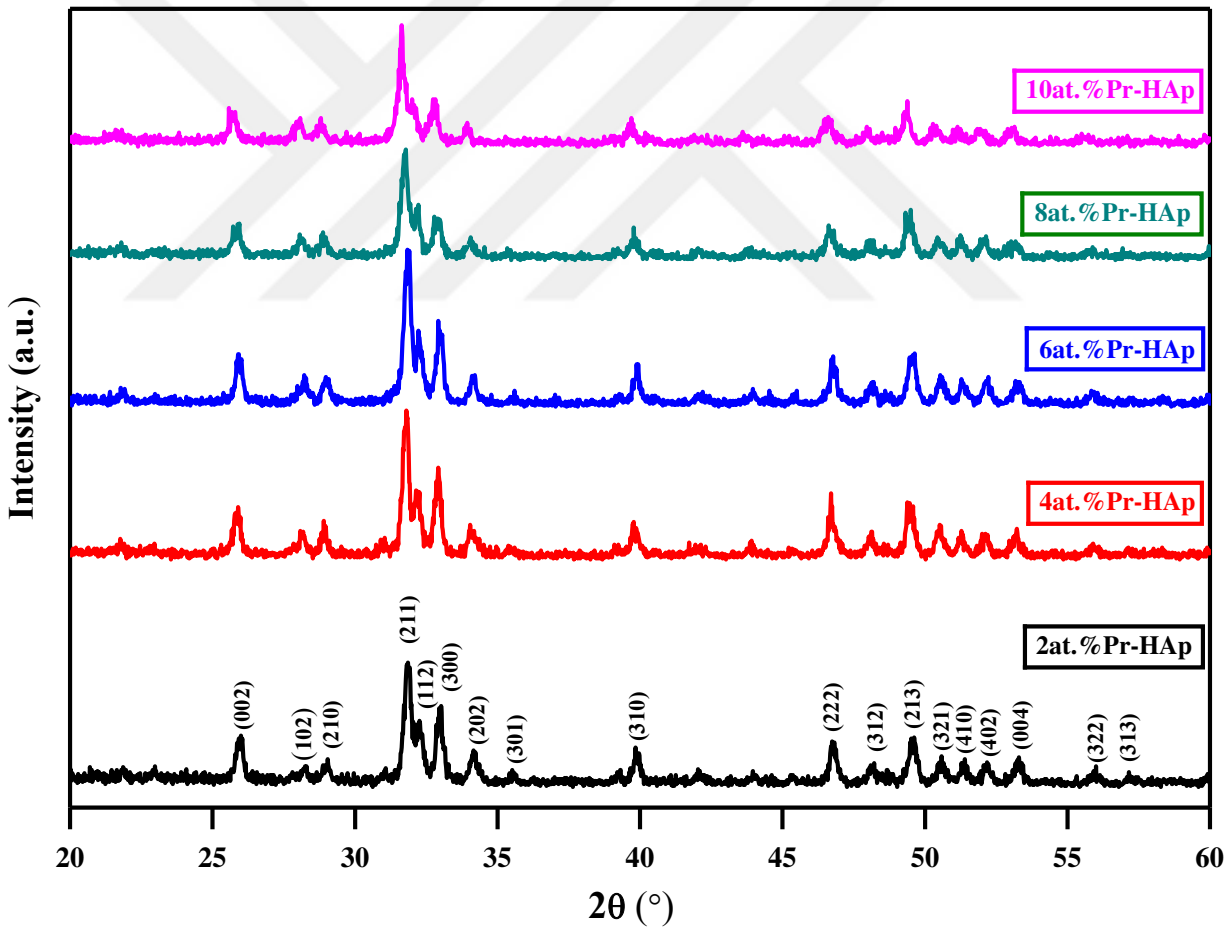

Figure 6.1. XRD patterns of Pr-doped Haps

The crystallite size values were calculated using the well-known method as proposed by Scherer (D_S) and Williamson-Hall (D_{WH}) formulas, respectively [65, 66]:

$$D_S = \frac{k\,\lambda}{\beta \cos\theta} \tag{6.1}$$

$$\beta \cos\theta = \frac{k\,\lambda}{D_{WH}} + 4\varepsilon \sin\theta \tag{6.2}$$

where D_S is crystallite size (nm), k is the shape factor (0.9), β is the full width at half maximum (in radians), λ is the X-rays wavelength, ε is the lattice strain, θ is the angle of Bragg diffraction (in degrees). The graphs of $\beta\cos\theta$ vs. $4\sin\theta$ for each sample are shown in Figure 6.2 can calculate the crystallite size by taking into account the lattice strain and defects, and the slope and y-intercept of these graphs give the lattice strain and crystallite size values, respectively. The lattice strain is affected by the dopants, and this parameter is positive (negative) when crystal lattice is under the effect of mechanical properties such as tensile (compressive) forces [67]. Moreover, with an increase in Pr content from 2 at.% to 4 at.%, the crystallite size increased and the lattice strain decreased as its value remained positive. For 6 at.% Pr-HAp, the crystallite size decreased, and the lattice strain increased. However, 8 at.% Pr-HAp the sign of the lattice strain was changed from positive to negative, and the crystallite size increased. In this regard, the 8 at.% Pr may be accepted as a critical content for the mechanical properties of HAp. The 10 at. % Pr–HAp has the biggest value of lattice strain, and there was the alteration in the sign of the lattice strain from negative to positive. Our results are in good agreement with Hossain et al. [68].

Lattice stress (σ) is proportional to the lattice strain(ε) with the constant of proportionality Young's modulus (Y), $\sigma = \varepsilon\, Y$. So, can be replaced by the ε factor in the second term of the Eq. (6.2) by $\varepsilon=\sigma/Y$ relation, and the modified equation is given by [65].

$$\beta \cos\theta = \frac{0.9\lambda}{D_{WH}} + \frac{4\sigma \sin\theta}{Y} \tag{6.3}$$

The slope of the graph between $\beta\cos\theta$ vs. $4\sin\theta Y^{-1}$ shown in Figure 6.3, gives the stress value (σ). Here Y is Young's modulus in the direction normal to the set of Miller indices ($h\,k\,l$) for each

crystal lattice plane detected on the XRD pattern can be calculated using the following relation for the hexagonal crystal structure [69].

$$Y = \frac{\left[h^2 + \frac{(h+2k)^2}{3} + \left(\frac{al}{c}\right)^2 \right]^2}{s_{11}\left(h^2 + \frac{(h+2k)^2}{3} \right)^2 + s_{33}\left(\frac{al}{c}\right)^4 + (2s_{13} + s_{44})\left(h^2 + \frac{(h+2k)^2}{3} \right)\left(\frac{al}{c}\right)^2} \qquad (6.3)$$

where a and c are represented the lattice parameters. s_{11}, s_{13}, $s_{33,}$ and s_{44} are the elastic compliance values and their standard values are reported as 7.49×10^{-12}, -4.0×10^{-12}, 10.9×10^{-12} and 15.1×10^{-12} m^2N^{-1}, respectively.

The anisotropic energy density (u) can be calculated according to Hook's law $u = \varepsilon^2 Y\ /2$, and therefore, the modified Eq. (6.2) can be replaced by the second term $(2u/Y)^{1/2}$ instead of ε is given by.

$$\beta\cos\theta = \frac{0.9\lambda}{D_{WH}} + 4\sin\theta\left(\frac{2u}{Y}\right)^{1/2} \qquad (6.4)$$

Hereby, the anisotropic energy (u) can be estimated from the slope of the $\beta\cos\theta$ vs. $2^{5/2}\sin\theta Y^{-1/2}$ plot as illustrated in Figure 6.4.

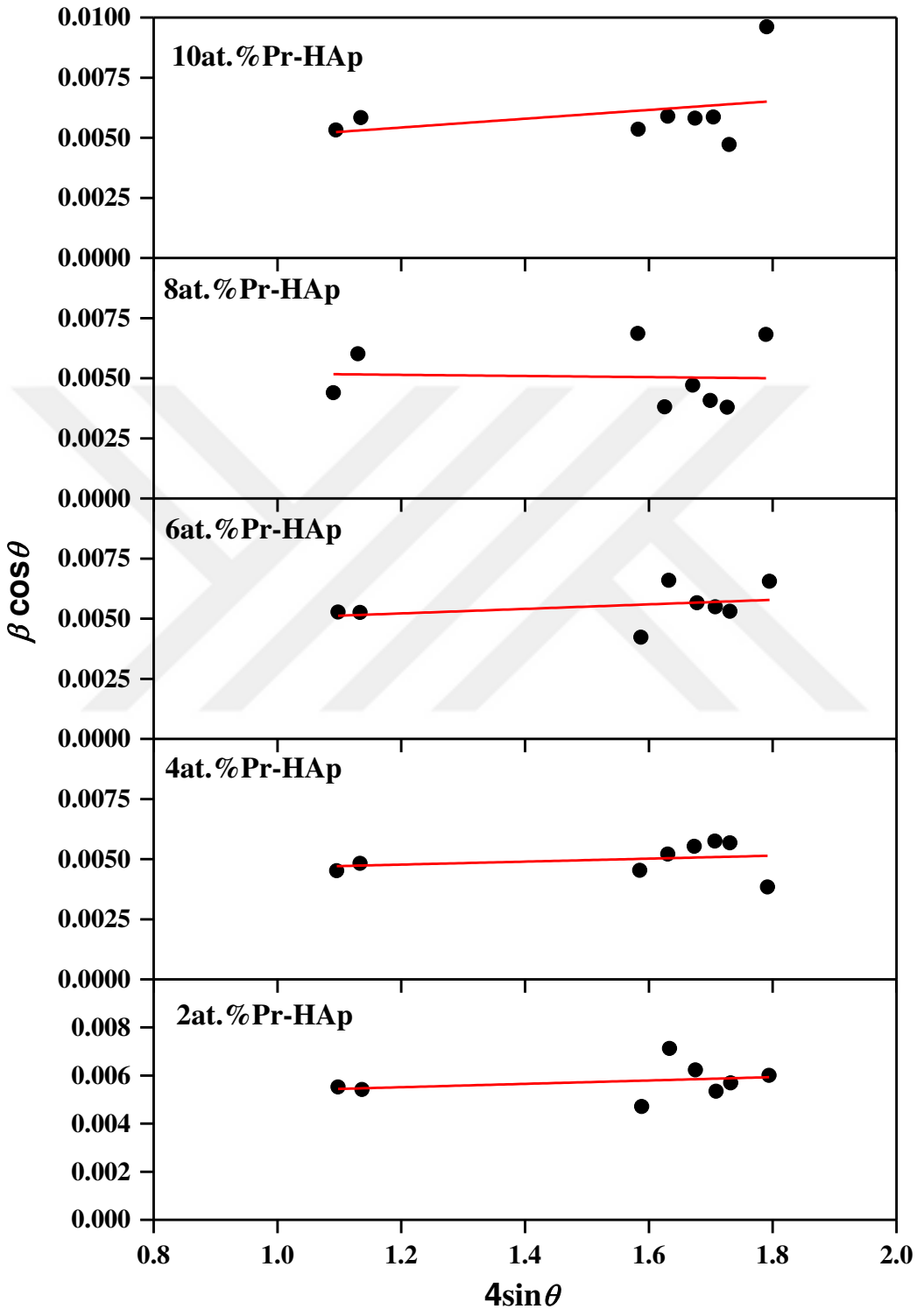

Figure 6.2. The $\beta cos\theta$ vs. $4\sin\theta$ plots of the as-synthesized Pr-doped HAps

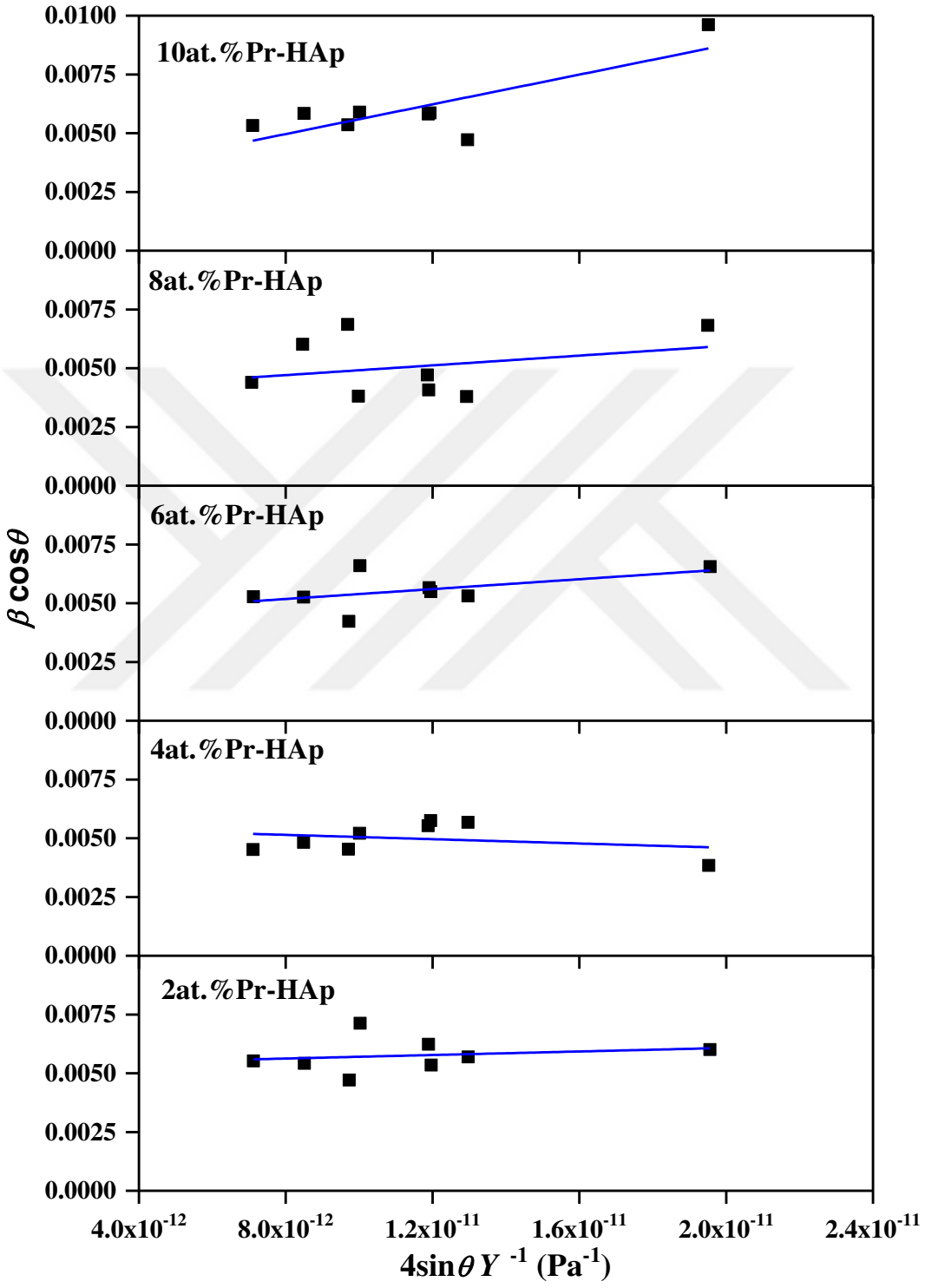

Figure 6.3. The $\beta cos\theta$ vs. $4\sin\theta\ Y^{-1}$ graphs of the as-prepared HAps

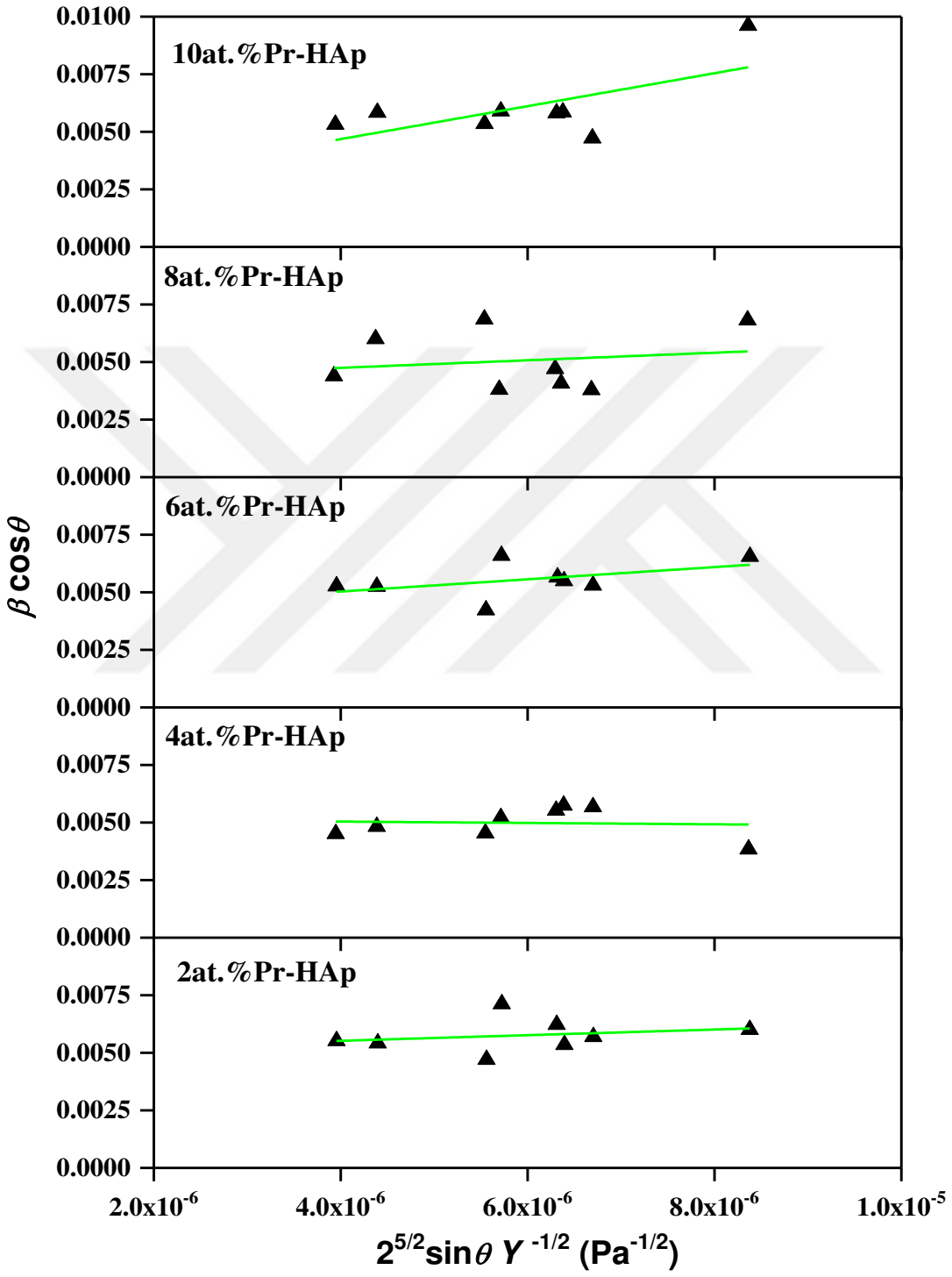

Figure 6.4. The $\beta cos\theta$ vs. $2^{5/2}\sin\theta\ Y^{-1/2}$ graphs for each sample

The lattice parameters of the HAp *a*- and *c*-axis (nm), the distance (nm) between adjacent planes, and unit cell volume (nm^3) for the hexagonal structure were calculated from all peaks of Miller indices (*h k l*) using the following relations, respectively [70].

$$\frac{1}{d^2} = \frac{4}{3}\left(\frac{h^2 + hk + k^2}{a^2}\right) + \frac{l^2}{c^2} \tag{6.5}$$

$$V = 0.866a^2c \tag{6.6}$$

Table 6.1. Experimental values of the XRD parameters

	Sample				
Parameter	**2at.% Pr-HAp**	**4at.% Pr-HAp**	**6at.% Pr-HAp**	**8at.% Pr-HAp**	**10at.% Pr-HAp**
D_S (nm)	25.59	28.78	26.39	29.23	31.53
D_{WH} (nm)	29.69	34.40	33.90	35.74	42.79
a (nm)	0.9403	0.9408	0.9421	0.9423	0.9445
c (nm)	0.6867	0.6866	0.6879	0.6879	0.6897
V (nm^3)	0.5258	0.5263	0.5287	0.5290	0.5328
X_C%	86.09	82.02	78.63	73.03	68.12
X_{CL}%	87.81	84.42	83.67	78.57	73.81
ε	0.700×10^{-3}	0.617×10^{-3}	0.944×10^{-3}	-0.238×10^{-3}	1.830×10^{-3}
σ (MPa)	37.539	-45.781	105.206	103.727	316.184
u (kJ m^{-3})	14.947	0.877	7.848	27.230	511.468

In addition, the as-calculated values of *a*, *c*, *V*, and X_C are shown in Table 6.1. Table 6.1 results show that both the lattice parameter and unit cell volume of Pr-HAp increased with the addition of Pr concentration, while the crystallinity decreased with increasing Pr in the Pr-HAp structure, due to a bit bigger dimensions of Pr^{3+} (0.0997 nm) than Ca^{2+} (0.099 nm). From Table 6.1, the observed crystallite size values were found to increase with Pr concentration increasing.

It should be noted here that according to Landi et al. [71] the percentage of crystallinity degree (X_{CL}%) for all samples were determined using the intensity of the trough between (112) and (300) reflections ($V_{112/300}$), and the intensity of (3 0 0) diffraction peak (I_{300}) as demonstrated in Figure 6.5.

$$X_{CL}\% = \left(1 - \frac{V_{112/300}}{I_{300}}\right) \times 100 \tag{6.7}$$

The crystallinity degree (*X*c%) value can also be calculated from Eq.(6.8).

$$X_C\% = \frac{\sum A_C}{\sum A_C + \sum A_A} \times 100 \tag{6.8}$$

where $\sum A_C$ is the total area under crystal peaks and $\sum A_A$ is the area under amorphous peaks [72].

The increase in the crystallite dimensions, lattice parameter *a* and unit cell volume was found with an increasing amount of Pr In addition, the lattice parameter *c* remained almost constant for all samples except the 10 at.% Pr-HAp one is a significant increase. However, the percentage of crystallinity decreased with the Pr amount increasing.

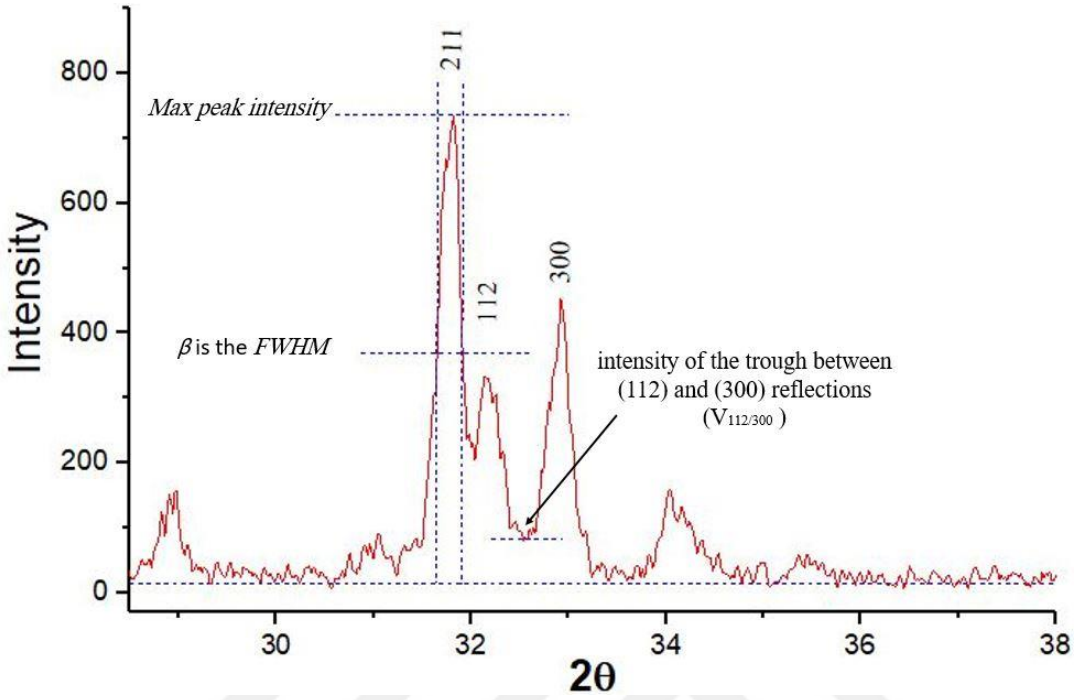

Figure 6.5. The FWHM peak intensity in the Scherrer's equation and the intensity of the troughs between (112) and (300) reflections ($V_{112/300}$)

6.2. FTIR Spectroscopic Analysis

Functional groups of all samples were investigated using the FTIR technique and the obtained spectra of the Pr doping HAp are shown in Figure 6.6. The vibration at 563 cm^{-1}, 600 cm^{-1}, and 632 cm^{-1} were assigned to the bending mode of PO_4^{3-} group, as well as the band at 962 cm^{-1} and 1089 cm^{-1}, were observed to the stretching mode of PO_4^{3-} group [73]. The spectra of the hydroxyl band have been magnified for all samples ranged from 3572 cm^{-1} 2 at.% Pr-HAp to 3570 cm^{-1} 10 at.% Pr-HAp, respectively. OH^- bending and stretching modes were also observed at 631 cm^{-1} and 3572 cm^{-1}, respectively. The spectra of OH^- stretching mode showed a shift towards the low value of vibration peak from 3572 cm^{-1} to 3570 cm^{-1} for 3572 cm^{-1} 2 at.% Pr-HAp to 3570 cm^{-1} 10 at.% Pr-HAp, respectively.

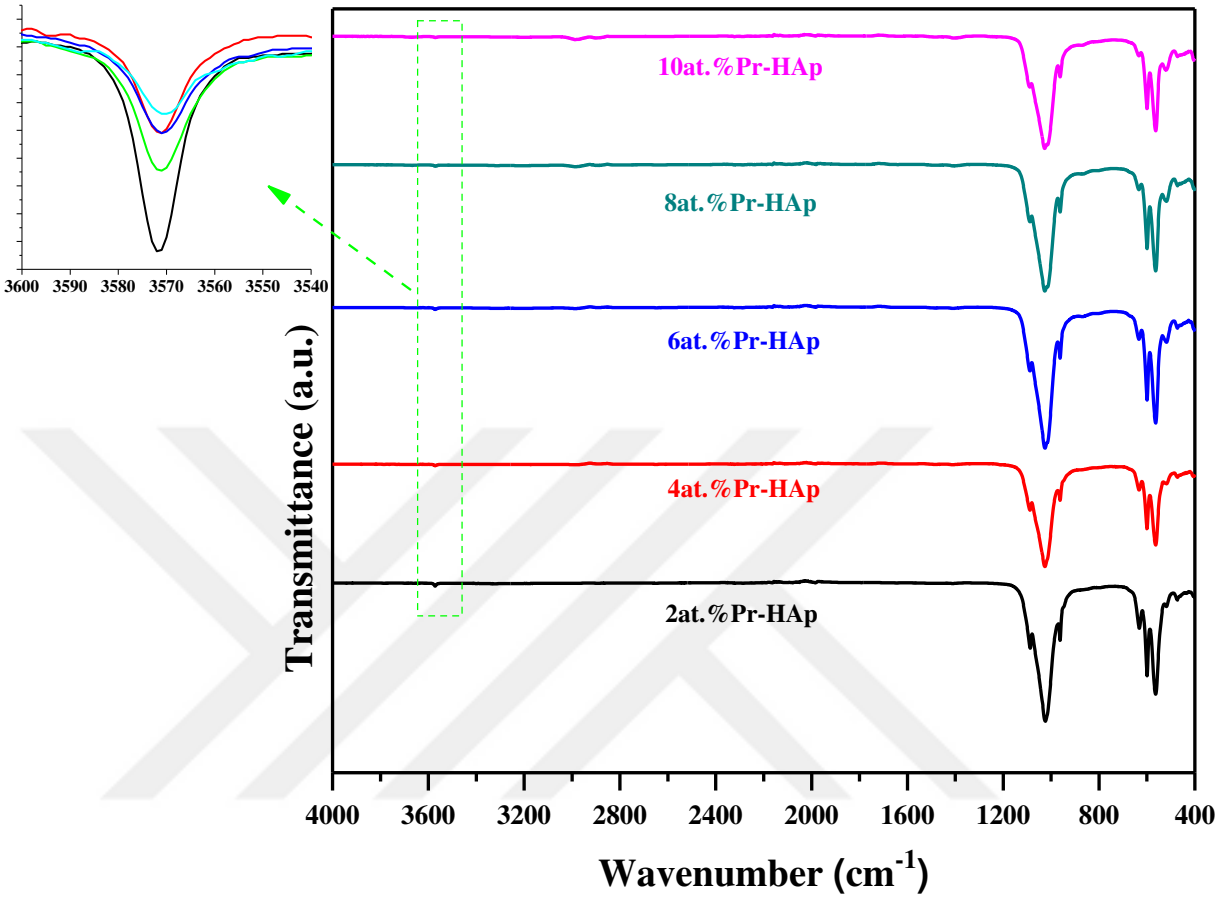

Figure 6.6. FTIR spectra of the as-prepared HAp samples

6.3. Morphological Studies

The scanning electron microscope (SEM) was used for the morphological study of samples of hydroxyapatite (HAp) doped with praseodymium (Pr). It was proved that the HAp grain indicated a non-uniform size and shape because of abnormal grain growth. Figure 6.7 illustrates the SEM images of all Pr-HAp samples. All the samples have bound and highly agglomerated particle morphology. The agglomeration of the nanoparticles might be because of Ostwald ripening.

According to the EDX results of Pr-HAp powders, O, P, Ca and Pr were observed and calculations of the amounts of these, have been engaged for each region where EDX analysis was performed as illustrated in Figure 6.7. No other impurities were detected. Furthermore, it is also observed that Ca was partly substituted with Pr. The molar ratios of (Ca+Pr)/P were calculated for each specimen and 2 at.% Pr-HAp, 4 at.% Pr-HAp, 6 at.% Pr-HAp, 8 at.% Pr-HAp, and 10 at.% Pr-HAp samples were found to have 1.63, 1.70, 1.73, 1.59, and 1.57, respectively. The molar ratios of Ca/P

were estimated to be 1.65, 1.65, 1.63, 1.48 and 1.42 for 2 at.% Pr-HAp, 4 at.% Pr-HAp, 6 at.% Pr-HAp, 8 at.% Pr-HAp, and 10 at.% Pr-HAp, respectively. These values are very nearby to the Ca/P ratio of the human bone [74]. Except for the 8 at.% Pr-HAp, and 10 at.% Pr-HAp samples. For both samples, these values indicate the Ca-deficiency.

6.4. Thermal Analysis Results

The DTA and TGA curves are shown in Figure 6.8 (a,b), respectively. Both methods are useful to determine the effects of Pr-doping on the thermal stability and mass change of HAp as a function of increasing temperature. There were no significant differences in DTA plots among the five compositions. As well as, the endothermic and exothermic peaks did not detect in the DTA curves of the as-prepared samples, and this implies that all the samples are thermally stable in the temperature interval of 25-1000 °C. It also appears that the amount of Pr used in this study did not significantly influence the thermal stability of the apatitic structure during the above-mentioned temperature period [30]. As well known, TGA is the measurement of the gain and loss of the mass of the samples with respect to temperature. The mass between 20 and 450 °C remained almost constant and gradually increased between 450 and 1000 °C as shown in Figure 6.8 b). This synthesis can be considered thermally stable as a sign that the amount of dopant used in this search did not affect significantly the thermal properties and these values are in good agreement with the typical values reported in the literature [75]. The maximum mass gain percentages of the samples in this temperature interval are found to be 1.54%, 2.08%, 1.20%, 1.19% and 1.25% for 2at. %Pr-HAp, 4at. %Pr-HAp, 6at. %Pr-HAp, 8at. %Pr-HAp, and 10at. %Pr-HAp, respectively.

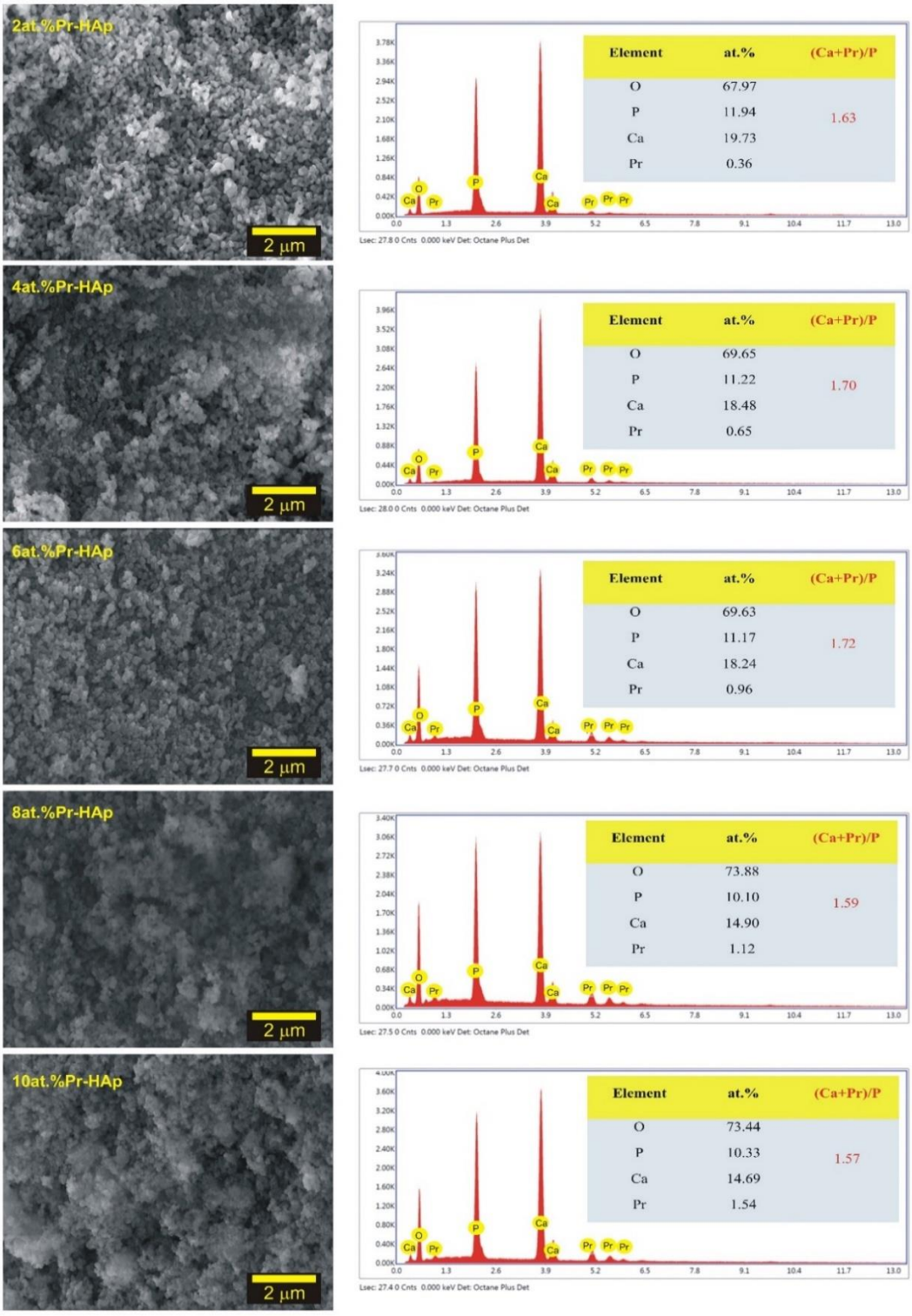

Figure 6.7. SEM micrographs and EDX report of the as-synthesized HAps

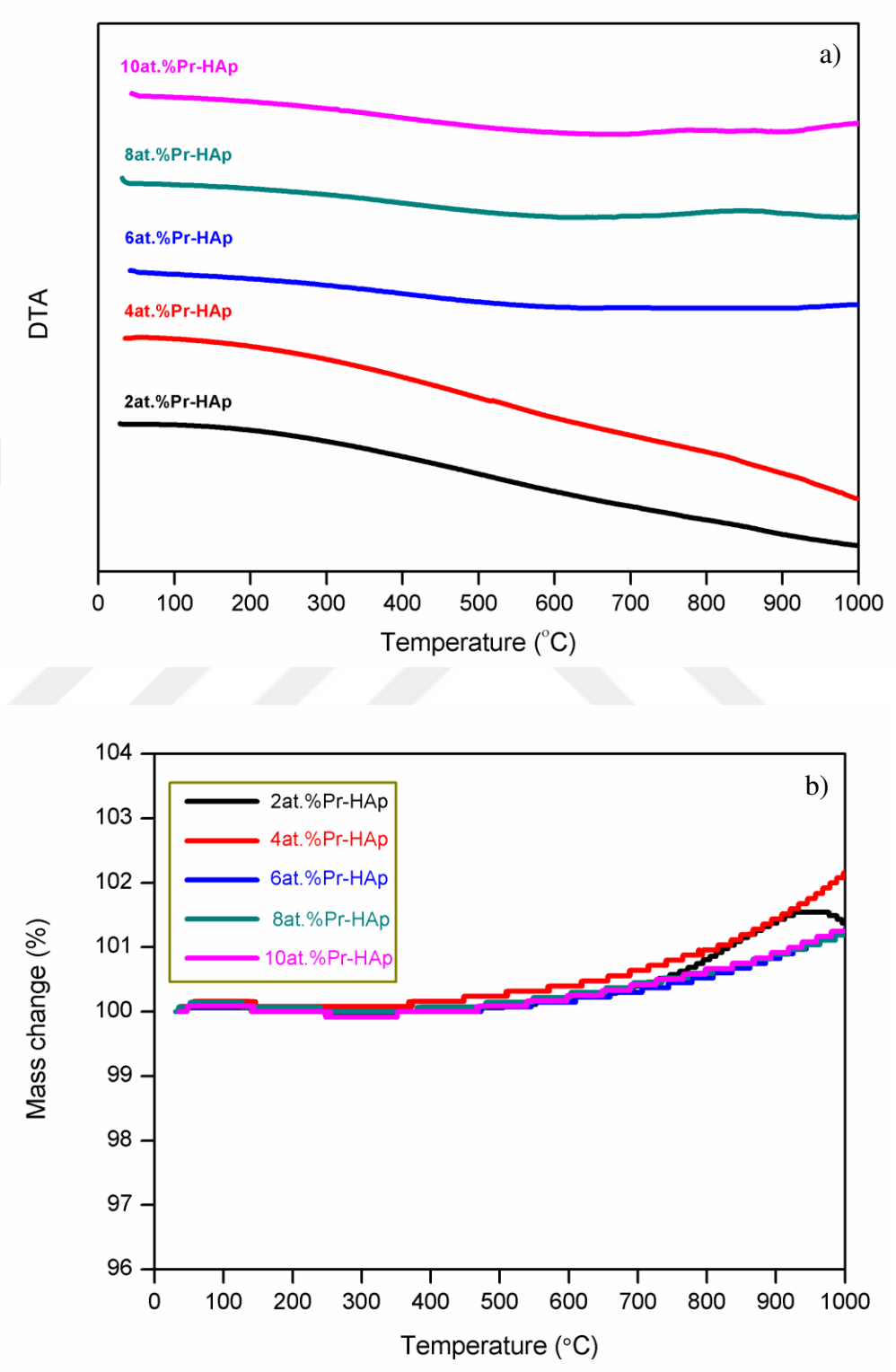

Figure 6.8. a) DTA and **b)** TGA curves of the as-prepared samples

6.5. Cytotoxicity Study

The cell viability results of the samples are shown in Figure 6.9. According to the test results, 2 at.% Pr-HAp, 4 at.% Pr-HAp, 6 at.% Pr-HAp, 8 at.% Pr-HAp, and 10 at.% Pr-HAp samples have 73.268±11.018, 72.536±14.291, 54.343±9.16, 82.018±13.416 and 95.361±12.511 percent of cell viability values with standard deviations compared to the control group, respectively. Thus, 6 at.% Pr–HAp has the lowest cell viability which means that it has the most cytotoxic effect over L-929 mouse fibroblast cells. On the other hand, having a cell viability value of higher than 95%, 10 at.% Pr–HAp is the most biocompatible material compared to the other samples. In addition, 2 at.% Pr–HAp and 4 at.% Pr–HAp samples have similar characteristics in terms of cell viability results. Depending on the cell viability results of the samples, our results show that 10 at.% Pr–HAp >8 at.% Pr–HAp >2 at.% Pr–HAp >4 at.% Pr–HAp >6 at.% Pr–HAp.

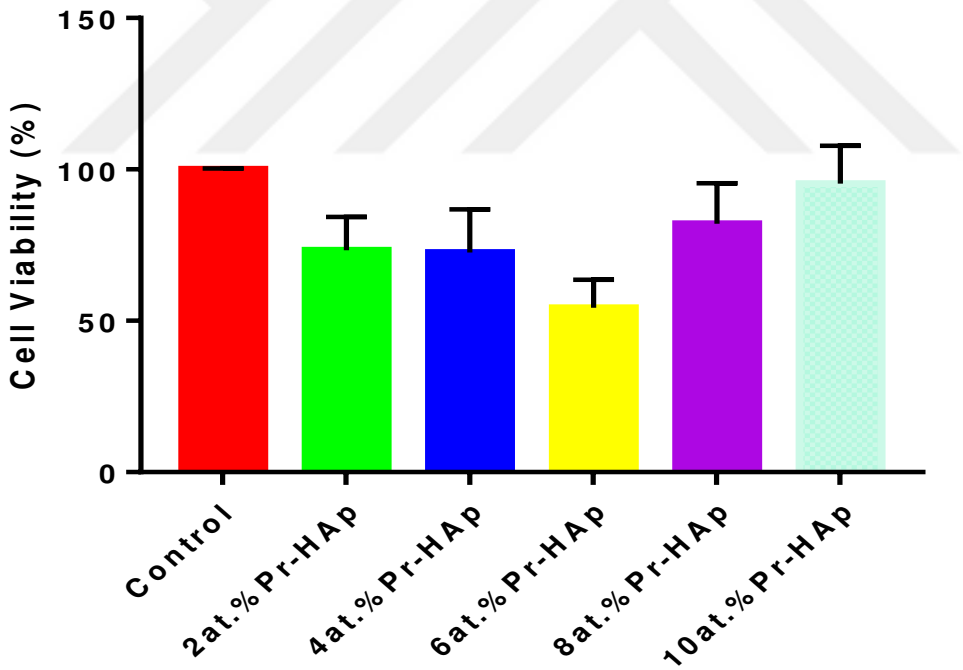

Figure 6.9. The cell viability results for each Pr-doped HAp sample

6.6. The Density of States and Band Structure

The density of states as a function of energy has been calculated as [76]

$$DOS\,(\mathrm{E}) = \sum {}^{\mathrm{g}}(\mathrm{E}\text{-}\varepsilon_{\mathrm{i}}) \tag{6.9}$$

where g is a Gaussian with fixed full-width-half-maximum (FWHM), ε_i is the energy of the i^{th} molecular orbital, and E is the total energy. Figure 6.10-Figure 6.14 demonstrates the band structure and density of states of the Pr doping HAp. All atomic calculations and simulations were analyzed using quantum espresso software package [77]. The energy band gap between Higher Occupied Molecular Orbital (HOMO), and Lower Unoccupied Molecular Orbital (LUMO) can be found by using density functional theory (DFT). The Pr doping HAp surfaces have a band gap between the top of the valence band (VB) and the bottom of the conduction band (CB), located at the K point. The band gap values of the samples were found to be 3.8199, 3.4139, 2.9667, 2.7791 and 1.3230 eV for 2 at.% Pr–HAp, 4 at.% Pr–HAp, 6 at.% Pr–HAp, 8 at.% Pr–HAp and 10 at.% Pr–HAp, respectively. All sample systems exhibit low-dispersive valence band top and conduction band bottom along with the line frequencies, imply that in this region the excitation energy occurs. This represents one of the most powerful features of optical adsorption [78]. The electron at the valence band edge absorbs energy and reaches the energy level of the CB edge through the energy band gap at (G-L) that displays the smallest energy band gap between the VB and CB. On the other hand, the VB minimum and CB maximum are located between (H-K) the shows almost flat, and their heavy holes imply relatively lower mobility. Another interesting feature the highest value of the band gap can be shown on the (H) point, indicating that the Pr–HAp molecule can be an indirect band gap material because the minimum and maximum of the energy take place at different wave vectors. According to results discovered that good agreement when comparing our method with typical results with Alexander et al. [79]. They conducted a computational study based on approximation density functional theory (DFT) using Perdew-Wang (PW91) software program to identify the electronic structure of pure HAp, they noticed that also the band structure of pure HAp is an indirect gap material.

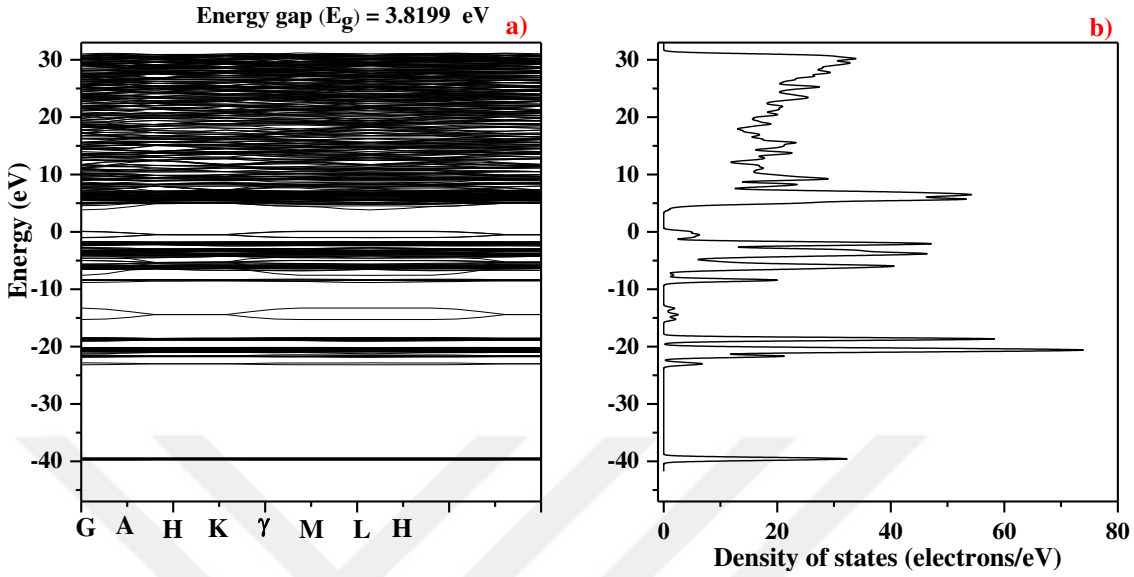

Figure 6.10. **a)** Band structure and **b)** density of states for 2at.%Pr–HAp

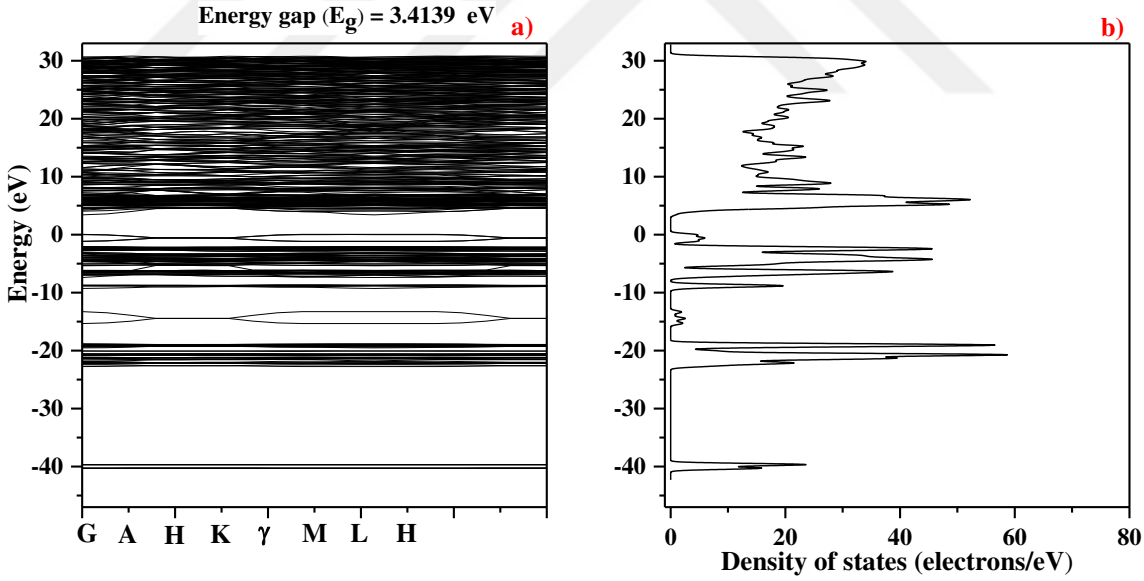

Figure 6.11. **a)** Band structure and **b)** density of states for 4at.%Pr–HAp

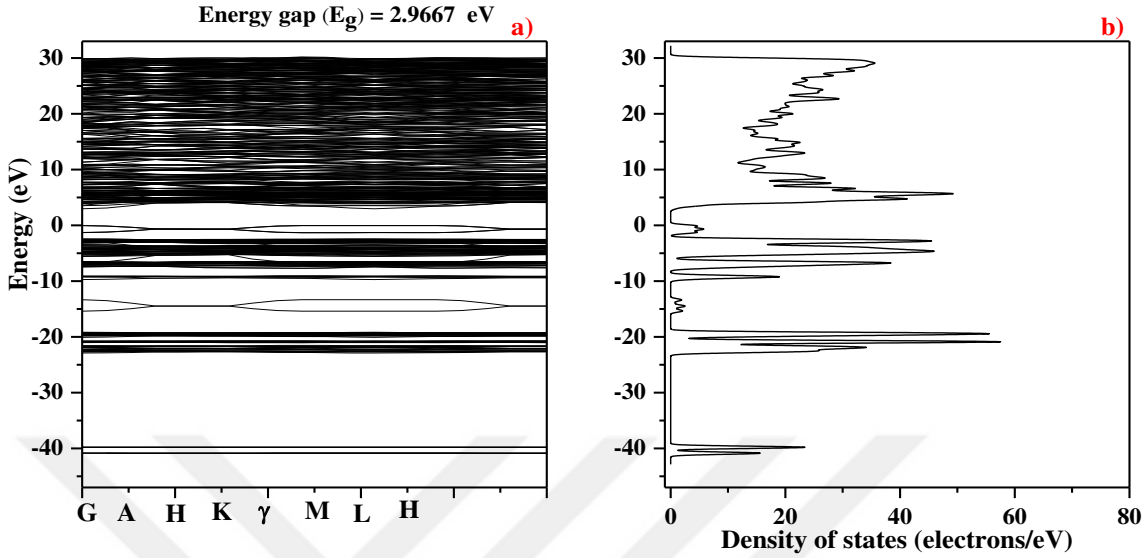

Figure 6.12. **a)** Band structure and **b)** density of states for 6at. %Pr–HAp

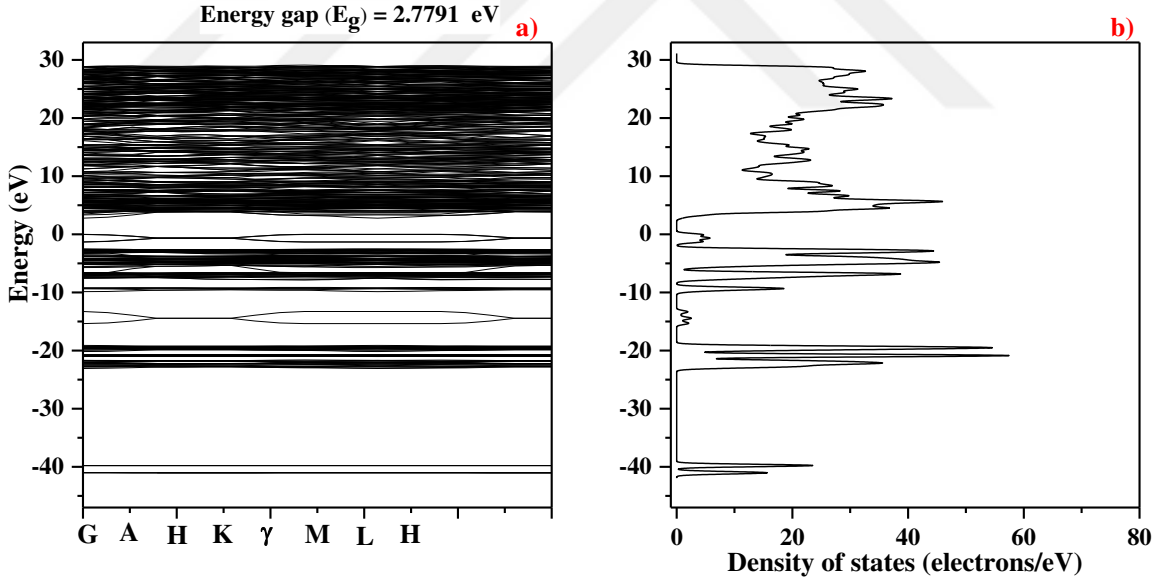

Figure 6.13. **a)** Band structure and **b)** density of states for 8at.%Pr–HAp

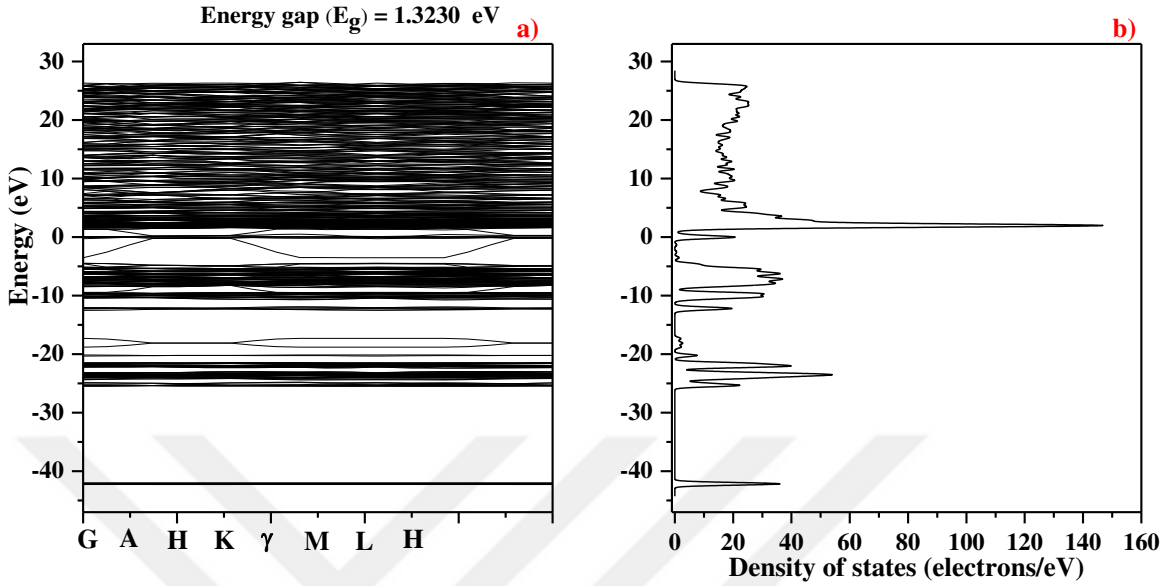

Figure 6.14. **a)** Band structure and **b)** density of states for 10at.%Pr–HAp

7. CONCLUSION

In the present work, we synthesized five hydroxyapatite (HAp) samples doped with praseodymium (Pr) at various amounts of 2, 4, 6, 8 and 10 at.% via using the wet chemical method at low temperature that can be confirmed by FT- IR, XRD, EDX, SEM, biocompatibility test, thermal stability. Besides, the samples were modeled by using the Quantum Espresso software and theoretically characterized by using the DFT. With the addition of Pr, the following findings can be reached. The influence of Pr-ions in HAp structure was detected.

From the XRD, FTIR and SEM results of Pr-HAp powder were observed synthesized successfully substituted Pr ions into the HAp crystal structure. The crystallite size calculated using Scherrer and Williamson-Hall formula was found to be in the range of ~25 – 31 nm, 29 – 42 nm, respectively. The lattice parameter *a* and the unit cell volume increased, while the crystallinity percent gradually decreased. The lattice parameter *c*, lattice strain, stress, and anisotropic energy values were affected by Pr content. No significant changes in the morphology were observed. The theoretical results showed that the band gap energy of HAp decreased steadily from 3.82 eV to 1.32 eV with adding of Pr and the DOS was also affected by Pr content. Furthermore, the electronic structure Pr–HAp molecule can be an indirect band gap material these agree well with pure HAp. Pr content in the range of 2 to 10 at.% did not affect the thermal stability of HAp. Except for the sample having 6 at.% Pr, all the remaining samples can be used for biological applications.

In summary, Pr-substituted HAp (Pr–HA) can be chosen as an appropriate candidate for biomedical applications due to as showed a biological study *in vitro* of the HAp powder, it elicits a favorable biological response.

REFERENCES

[1] Stone, A.R.. (1996). *The war of desire and technology at the close of the mechanical age*. MIT press.

[2] Ratner, B.D., Hoffman, A.S., Schoen, F.J., and Lemons, J.E**.** (2006). *Biomaterials science: an introduction to materials in medicine*. MRS Bull, 31, 59.

[3] Suchanek, W. and Yoshimura, M. (1998). Processing and properties of hydroxyapatite-based biomaterials for use as hard tissue replacement implants. *Journal of Materials Research*, 13(1), 94-117.https://doi.org/10.1557/JMR.1998.0015

[4] Ratner, B.D.(1996). *Biomaterials science: an interdisciplinary endeavor*. Biomaterials Science, Elsevier. p. 1-8. https://doi.org/10.1016/B978-0-08-050014-0.50005-5

[5] Rho, J.-Y., Kuhn-Spearing, L., and Zioupos, P. (1998). Mechanical properties and the hierarchical structure of bone. *Medical engineering & physics*, 20(2), 92-102. https://doi.org/10.1016/S1350-4533(98)00007-1

[6] Sandhu, G.S., 2010. *Synthesis and characterization of microspheres for controlled release*.MSc thesis. Missouri University of Science and Technology

[7] Park, J.B. and Bronzino, J.D. (2002). *Biomaterials: principles and applications*, CRC Press.

[8] Marks Jr, S.C. and Odgren, P.R.(2002). *Structure and development of the skeleton, in Principles of bone biology*. Elsevier. p. 3-15. https://doi.org/10.1016/B978-012098652-1.50103-7

[9] Martini, F.H., Nath, J., and Bartholomew, E. (1998). *Fundamentals of Anatomy and Physiology*. ed, PEI San Franciso2006.

[10] Williams, D.F.(1999). *The Williams dictionary of biomaterials*, Liverpool University Press.

[11] Gibson, I., Akao, M., Best, S., and Bonfield, W. (1996). Phase transformations of tricalcium phosphates using high temperature X-ray diffraction. Proceedings of the 9th International Symposium on Ceramics in Medicine.Quintessence Publication. 173-176

[12] Shirwaiker, R., Purser, M., and Wysk, R. (2014). *Scaffolding hydrogels for rapid prototyping based tissue engineering*, in *Rapid Prototyping of Biomaterials*. Elsevier. p. 176-200. https://doi.org/10.1533/9780857097217.176

[13] Vallet-Regí, M., Pena, J., and Izquierdo-Barba, I. (2004). Synthesis of β-tricalcium phosphate in layered or powdered forms for biomedical applications. *Solid State Ionics*, 172(1-4), 445-449. https://doi.org/10.1016/j.ssi.2004.04.038

[14] Zyman, Z.Z., Rokhmistrov, D.V., and Loza, K.I. (2013). Determination of the Ca/P ratio in calcium phosphates during the precipitation of hydroxyapatite using X-ray diffractometry. *Process and Appl Ceramics*, 7, 93-95. DOI: 10.2298/PAC1302093Z

[15] Sherin, S., Sheeja, S., Devi, R.S., Balachandran, S., Soumya, R.S., and Abraham, A. (2017). In vitro and in vivo pharmacokinetics and toxicity evaluation of curcumin incorporated titanium dioxide nanoparticles for biomedical applications. *Chemico-biological interactions*, 275, 35-46. https://doi.org/10.1016/j.cbi.2017.07.022

[16] Davis, J. (2003). *Overview of biomaterials and their use in medical devices*. Handbook of materials for medical devices, 1-11.

[17] Chetty, A., Wepener, I., Marei, M.K., Kamary, Y., and Moussa, R.M. (2012) *Synthesis, properties, and applications of hydroxyapatite*. Nova Science Publishers.

[18] Bohner, M. (2000). Calcium orthophosphates in medicine: from ceramics to calcium phosphate cements. *Injury*, 31, D37-D47. https://doi.org/10.1016/S0020-1383(00)80022-4

[19] Dorozhkin, S. (2009). Calcium orthophosphates in nature, biology and medicine. *Materials*, 2(2), 399-498. https://doi.org/10.3390/ma2020399

[20] Gauthier, O., Goyenvalle, E., Bouler, J.-M., Guicheux, J., Pilet, P., Weiss, P., and Daculsi, G. (2001). Macroporous biphasic calcium phosphate ceramics versus injectable bone substitute: a comparative study 3 and 8 weeks after implantation in rabbit bone. *Journal of materials science: materials in medicine*, 12(5), 385-390.

[21] De Jong, W. (1926). La substance minerale dans les os. *Recueil des Travaux Chimiques des Pays-Bas*, 45(6), 445-448. https://doi.org/10.1002/recl.19260450613

[22] Ezhaveni, S., Yuvakkumar, R., Rajkumar, M., Sundaram, N.M., and Rajendran, V. (2013). Preparation and characterization of nano-hydroxyapatite nanomaterials for liver cancer cell treatment. *Journal of nanoscience and nanotechnology*, 13(3), 1631-1638. https://doi.org/10.1166/jnn.2013.7135

[23] Rivera-Muñoz, E.M. (2011). Hydroxyapatite-based materials: synthesis and characterization. *Biomedical Engineering-Frontiers and Challenges*.Croatia 75-99.

[24] Šupová, M. 2(015). Substituted hydroxyapatites for biomedical applications: a review. *Ceramics international*, 41(8), 9203-9231. https://doi.org/10.1016/j.ceramint.2015.03.316

[25] Hench, L.L. (1991). Bioceramics: from concept to clinic. *Journal of the american ceramic society*, 74(7), 1487-1510. https://doi.org/10.1111/j.1151-2916.1991.tb07132.x

[26] Park, J. (2009). *Bioceramics: properties, characterizations, and applications*. Springer Science & Business Media.

[27] Dorozhkin, S.V. and Epple, M. (2002). Biological and medical significance of calcium phosphates. *Angewandte Chemie International Edition*, 41(17), 3130-3146. https://doi.org/10.1002/1521-3773(20020902)41:17<3130::AID-ANIE3130>3.0.CO;2-1

[28] Weiner, S. and Wagner, H.D. (1998). The material bone: structure-mechanical function relations. *Annual review of materials science*. 28(1), 271-298. https://doi.org/10.1146/annurev.matsci.28.1.271

[29] Sadat-Shojai, M., Khorasani, M.-T., Dinpanah-Khoshdargi, E., and Jamshidi, A. (2013). Synthesis methods for nanosized hydroxyapatite with diverse structures. *Acta biomaterialia*, 9(8), 7591-7621. https://doi.org/10.1016/j.actbio.2013.04.012

[30] İnce, T., Kaygili, O., Tatar, C., Bulut, N., Koytepe, S., and Ates, T. (2018). The effects of Ni-addition on the crystal structure, thermal properties and morphology of Mg-based hydroxyapatites synthesized by a wet chemical method. *Ceramics international*, 44(12), 14036-14043. https://doi.org/10.1016/j.ceramint.2018.04.257

[31] Donglu, S. (2005). *Introduction to biomaterials*. World Scientific.

[32] Hahn, B.-D., Lee, J.-M., Park, D.-S., Choi, J.-J., Ryu, J., Yoon, W.-H., Lee, B.-K., Shin, D.-S., and Kim, H.-E. (2010). Aerosol deposition of silicon-substituted hydroxyapatite coatings for biomedical applications. *Thin Solid Films*, 518(8), 2194-2199. https://doi.org/10.1016/j.tsf.2009.09.024

[33] Aminian, A., Solati-Hashjin, M., Samadikuchaksaraei, A., Bakhshi, F., Gorjipour, F., Farzadi, A., Moztarzadeh, F., and Schmücker, M. (2011). Synthesis of silicon-substituted hydroxyapatite by a hydrothermal method with two different phosphorous sources. *Ceramics international*, 37(4), 1219-1229. https://doi.org/10.1016/j.ceramint.2010.11.044

[34] Bang, L., Ishikawa, K., and Othman, R. (2011). Effect of silicon and heat-treatment temperature on the morphology and mechanical properties of silicon-substituted hydroxyapatite. *Ceramics international*, 37(8), 3637-3642. https://doi.org/10.1016/j.ceramint.2011.06.023

[35] Balamurugan, A., Rebelo, A., Lemos, A., Rocha, J., Ventura, J., and Ferreira, J. (2008). Suitability evaluation of sol–gel derived Si-substituted hydroxyapatite for dental and maxillofacial applications through in vitro osteoblasts response. *Dental Materials*, 24(10), 1374-1380. https://doi.org/10.1016/j.dental.2008.02.017

[36] Rajabi-Zamani, A., Behnamghader, A., and Kazemzadeh, A. (2008). Synthesis of nanocrystalline carbonated hydroxyapatite powder via nonalkoxide sol–gel method. *Materials Science and Engineering: C*, 28(8), 1326-1329. https://doi.org/10.1016/j.msec.2008.02.001

[37] Roche, K.J. and Stanton, K.T. (2014). Measurement of fluoride substitution in precipitated fluorhydroxyapatite nanoparticles. *Journal of Fluorine Chemistry*, 161, 102-109. https://doi.org/10.1016/j.jfluchem.2014.02.007

[38] Alshemary, A.Z., Goh, Y.-F., Akram, M., Razali, I.R., Kadir, M.R.A., and Hussain, R. (2013). Microwave assisted synthesis of nano sized sulphate doped hydroxyapatite. *Materials Research Bulletin*, 48(6), 2106-2110. https://doi.org/10.1016/j.materresbull.2013.02.015

[39] Tamm, T. and Peld, M. (2006). Computational study of cation substitutions in apatites, *Journal of Solid State Chemistry*, 179(5), 1581-1587. https://doi.org/10.1016/j.jssc.2006.02.012

[40] Lin, K., Liu, P., Wei, L., Zou, Z., Zhang, W., Qian, Y., Shen, Y., and Chang, J. (2013). Strontium substituted hydroxyapatite porous microspheres: surfactant-free hydrothermal synthesis, enhanced biological response and sustained drug release. *Chemical Engineering Journal*, 222, 49-59. https://doi.org/10.1016/j.cej.2013.02.037

[41] Kaygili, O., Keser, S., Bulut, N., and Ates, T. (2018). Characterization of Mg-containing hydroxyapatites synthesized by combustion method. *Physica B: Condensed Matter*, 537, 63-67. https://doi.org/10.1016/j.physb.2018.02.007

[42] Ren, F., Leng, Y., Xin, R., and Ge, X. (2010). Synthesis, characterization and ab initio simulation of magnesium-substituted hydroxyapatite. *Acta biomaterialia*, 6(7), 2787-2796. https://doi.org/10.1016/j.actbio.2009.12.044

[43] Zyman, Z., Tkachenko, M., Epple, M., Polyakov, M., and Naboka, M. (2006). Magnesium-substituted hydroxyapatite ceramics. *Materialwissenschaft und Werkstofftechnik: Entwicklung, Fertigung, Prüfung, Eigenschaften und Anwendungen technischer Werkstoffe*, 37(6), 474-477. https://doi.org/10.1002/mawe.200600022

[44] Sogo, Y., Sakurai, T., Onuma, K., and Ito, A. (2002). The most appropriate (Ca+ Zn)/P molar ratio to minimize the zinc content of ZnTCP/HAP ceramic used in the promotion of bone formation. *Journal of Biomedical Materials Research: An Official Journal of The Society for Biomaterials, The Japanese Society for Biomaterials, and The Australian Society for Biomaterials and the Korean Society for Biomaterials*, 62(3), 457-463. https://doi.org/10.1002/jbm.10200

[45] Ofudje, E.A., Adeogun, A.I., Idowu, M.A., and Kareem, S.O. (2019). Synthesis and characterization of Zn-Doped hydroxyapatite: scaffold application, antibacterial and bioactivity studies. *Heliyon*, 5(5), e01716 https://doi.org/10.1016/j.heliyon.2019.e01716.

[46] Miyaji, F., Kono, Y., and Suyama, Y. (2005). Formation and structure of zinc-substituted calcium hydroxyapatite. *Materials Research Bulletin*, 40(2), 209-220. https://doi.org/10.1016/j.materresbull.2004.10.020

[47] Basar, B., Tezcaner, A., Keskin, D., and Evis, Z. (2010). Improvements in microstructural, mechanical, and biocompatibility properties of nano-sized hydroxyapatites doped with yttrium and fluoride. *Ceramics international*, 36(5), 1633-1643. https://doi.org/10.1016/j.ceramint.2010.02.033

[48] Sakae, T., Ookubo, A., LeGeros, R.Z., Shimogoryou, R., Sato, Y., Lin, S., Yamamoto, H., and Kozawa, Y. *Bone formation induced by several carbonate-and fluoride-containing apatite implanted in dog mandible*. in *Key Engineering Materials*. 2003. Trans Tech Publ.

[49] Wieszczycka, K., Staszak, K., Woźniak-Budych, M.J., and Jurga, S. (2019). Lanthanides and tissue engineering strategies for bone regeneration. *Coordination Chemistry Reviews*, 388, 248-267. https://doi.org/10.1016/j.ccr.2019.03.003

[50] Massari, S. and Ruberti, M. (2013). Rare earth elements as critical raw materials: Focus on international markets and future strategies. *Resources Policy*, 38(1), 36-43. https://doi.org/10.1016/j.resourpol.2012.07.001

[51] Lu, Y. and Wang, E. (2010). *Rare Earth Polyoxometalate Complexes*, *Rare Earth Coordination Chemistry: Fundamentals and Applications*. John Wiley & Sons Singapore. p. 193-223.

[52] Vidaud, C., Bourgeois, D., and Meyer, D. (2012). Bone as target organ for metals: the case of f-elements. *Chemical research in toxicology*, 25(6), 1161-1175. https://doi.org/10.1021/tx300064m

[53] Bhanjadeo, M.M. and Subudhi, U. (2019). Praseodymium promotes B–Z transition in self-assembled DNA nanostructures. *RSC Advances*, 9(8), 4616-4620. DOI: 10.1039/C8RA10164G

[54] Mokoena, P.P. (2014). *Narrowband Ultraviolet B emission from gadolinium and praseodymium co-activated calcium phosphate phosphors for phototherapy lamps*. University of the Free State.

[55] Zamani, H.A., Arvinfar, A., Rahimi, F., Imani, A., Ganjali, M.R., and Meghdadi, S. (2011). Praseodymium analysis in aqueous solution by Pr3+–PVC membrane sensor based on N, N′-bis (4-hydroxysalicylidene)-1-3-phenylenediamine. *Materials Science and Engineering: C*, 31(2), 307-312. https://doi.org/10.1016/j.msec.2010.09.016

[56] Fricker, S.P. (2006). The therapeutic application of lanthanides. *Chemical Society Reviews*, 35(6), 524-533. DOI:10.1039/B509608C

[57] Sastri, V.R., Perumareddi, J., Rao, V.R., Rayudu, G., and Bünzli, J.-C. (2003). *Modern aspects of rare earths and their complexes*. Elsevier.

[58] Desai, A.Y. (2007). *Fabrication and characterization of titanium-doped hydroxyapatite thin films*. University of Cambridge. https://doi.org/10.17863/CAM.14178

[59] Tu, K.N., Lie, J.D., Wan, C.K.V., Cameron, M., Austel, A.G., Nguyen, J.K., Van, K., and Hyun, D. (2018). Osteoporosis: a review of treatment options. *Pharmacy and Therapeutics*, 43(2), 92.

[60] Liu, M., Xu, J., Tanswell, A.K., and Post, M. (1994). Inhibition of mechanical strain- induced fetal rat lung cell proliferation by gadolinium, a stretch- activated channel blocker. *Journal of cellular physiology*, 161(3), 501-507. https://doi.org/10.1002/jcp.1041610313

[61] Aissa, A., Debbabi, M., Gruselle, M., Thouvenot, R., Flambard, A., Gredin, P., Beaunier, P., and Tõnsuaadu, K. (2009). Sorption of tartrate ions to lanthanum (III)-modified calcium fluor-and hydroxyapatite. *Journal of Colloid and Interface Science*, 330(1), 20-28. https://doi.org/10.1016/j.jcis.2008.10.043

[62] Yasukawa, A., Gotoh, K., Tanaka, H., and Kandori, K. (2012). Preparation and structure of calcium hydroxyapatite substituted with light rare earth ions. *Colloids and Surfaces A: Physicochemical and Engineering Aspects*, 393, 53-59. https://doi.org/10.1016/j.colsurfa.2011.10.024

[63] Weekes, D., Cawthray, J., Rieder, M., Syeda, J., Ali, M., Wasan, E., Kostelnik, T., Patrick, B., Panahifar, A., and Al-Dissi, A. (2017). La (III) biodistribution profiles from intravenous and oral dosing of two lanthanum complexes, La (dpp) 3 and La (XT), and evaluation as treatments for bone resorption disorders. *Metallomics*, 9(7), 902-909. DOI:10.1039/C7MT00133A

[64] Serret, A., Cabanas, M.V., and Vallet-Regi, M. (2000). Stabilization of calcium oxyapatites with lanthanum (III)-created anionic vacancies. *Chemistry of Materials*, 12(12), 3836-3841. https://doi.org/10.1021/cm001117p

[65] Mansour, S., El-Dek, S., Dorozhkin, S., and Ahmed, M. (2017). Physico-mechanical properties of Mg and Ag doped hydroxyapatite/chitosan biocomposites. *New Journal of Chemistry*, 41(22), 13773-13783. DOI:10.1039/C7NJ01777D

[66] Yogamalar, R., Srinivasan, R., Vinu, A., Ariga, K., and Bose, A.C. (2009). X-ray peak broadening analysis in ZnO nanoparticles. *Solid State Communications*, 149(43-44), 1919-1923. https://doi.org/10.1016/j.ssc.2009.07.043

[67] Croft, M., Zhong, Z., Jisrawi, N., Zakharchenko, I., Holtz, R., Skaritka, J., Fast, T., Sadananda, K., Lakshmipathy, M., and Tsakalakos, T. (2005). Strain profiling of fatigue crack overload effects using energy dispersive X-ray diffraction. *International Journal of Fatigue*, 27(10-12), 1408-1419. https://doi.org/10.1016/j.ijfatigue.2005.06.022

[68] Moghaddam, H.M. and Nasirian, S. (2012). Dependence of activation energy and lattice strain on TiO 2 nanoparticles?. *Nanoscience Methods*, 1(1), 201-212. https://doi.org/10.1080/17458080.2011.620023

[69] Venkateswarlu, K., Bose, A.C., and Rameshbabu, N. (2010). X-ray peak broadening studies of nanocrystalline hydroxyapatite by Williamson–Hall analysis. *Physica B: Condensed Matter*, 405(20), 4256-4261. https://doi.org/10.1016/j.physb.2010.07.020

[70] Cullity, B.D. (1978). *Elements of X-ray diffraction, Addison*. Wesley Mass.

[71] Landi, E., Tampieri, A., Celotti, G., and Sprio, S. (2000). Densification behaviour and mechanisms of synthetic hydroxyapatites. *Journal of the European Ceramic Society*, 20(14-15), 2377-2387. https://doi.org/10.1016/S0955-2219(00)00154-0

[72] Kaygili, O. and Tatar, C. (2012)ceramics prepared by sol–gel method. *Journal of sol-gel science and technology*, 61(2), 296-309. DOI 10.1007/s10971-011-2627-0

[73] Lijuan, X., Liuyun, J., Lixin, J., and Chengdong, X. (2013). Synthesis of Mg-substituted hydroxyapatite nanopowders: effect of two different magnesium sources. *Materials Letters*, 106, 246-249. https://doi.org/10.1016/j.matlet.2013.05.032

[74] Trommer, R., Santos, L., and Bergmann, C. (2007). Alternative technique for hydroxyapatite coatings. *Surface and Coatings Technology*, 201(24), 9587-9593. https://doi.org/10.1016/j.surfcoat.2007.04.028

[75] Kaygili, O. (2019). Synthesis and characterization of Fe-containing biphasic calcium phosphate ceramics. *Journal of the Australian Ceramic Society*, 55(2), 381-385. https://doi.org/10.1007/s41779-018-0245-9

[76] Kebiroglu, M.H., Orek, C., Bulut, N., Kaygili, O., Keser, S., and Ates, T., 2017. Temperature dependent structural and vibrational properties of hydroxyapatite: A theoretical and experimental study, *Ceramics international*, 43(17), 15899-15904.

[77] Giannozzi, P., Baroni, S., Bonini, N., Calandra, M., Car, R., Cavazzoni, C., Ceresoli, D., Chiarotti, G.L., Cococcioni, M., and Dabo, I., 2009. QUANTUM ESPRESSO: a modular and open-source software project for quantum simulations of materials, *Journal of physics: Condensed matter*, 21(39), 395502.

[78] Avakyan, L.A., Paramonova, E.V., Coutinho, J., Öberg, S., Bystrov, V.S., and Bugaev, L.A. (2018). Optoelectronics and defect levels in hydroxyapatite by first-principles. *The Journal of chemical physics*, 148(15), 154706. https://doi.org/10.1063/1.5025329

[79] Slepko, A. and Demkov, A.A. (2011). First-principles study of the biomineral hydroxyapatite. *Physical Review B*, 84(13), 134108. https://doi.org/10.1103/PhysRevB.84.134108

CURRICULUM VITAE

Name: Riyadh Saeed
Surname: AGID
Date of Birth: 27-May-1988
Place of Birth: Mosul
Nationality: Iraq
E-mail: riyadh.physics88@gmail.com
Address: Salahaddin University

Education information:

The B.S. degree: Salahaddin University, College of Science, Physics Department (2013)

High school: Al-Ikhwa High School, Erbil, 2008

International Congress Presentations:

1) Riyadh Saeed Agid, Omer Kaygili, Niyazi Bulut, **A Detailed X-ray diffraction characterization of mg-substituted**, Oral Presentation, International Conference on Physical Chemistry and Functional Materials (PCFM'18), 2018.

2) Riyadh Saeed Agid, Omer Kaygili, Bayram Gunduz, Ismail Ercan, **A morphological analysis of nanostructured ZnO powder**, Poster Presentation, International Conference on Physical Chemistry and Functional Materials (PCFM'18), 2018.

3) Riyadh Saeed Agid, Ismail Ercan, Omer Kaygili, **An X-ray diffraction analysis of MgO samples by combustion method,** Poster Presentation, International Conference on Physical Chemistry and Functional Materials (PCFM'18), 2018.

4) Turan İnce, Serdar Acar, Ibrahim Isah Nasidi, Hanifi Kebiroglu, Bahroz Kareem Mahmood, **Riyadh Saeed Agid**, Lale Ibrahimzade, Tankut Ates, Niyazi Bulut, Omer Kaygili, **An X-Ray Diffraction Study of Mn-doped Hydroxyapatite**, Oral Presentation, Anadolu Kongreleri 3. Uluslararası Uygulamalı Bilimler Kongresi, pp. 401-402, 28-29 December 2019, Diyarbakır, Turkey. http://lnnk.in/WEi

5) Turan İnce, Serdar Acar, Ibrahim Isah Nasidi, Hanifi Kebiroglu, Bahroz Kareem Mahmood, **Riyadh Saeed Agid**, Lale Ibrahimzade, Tankut Ates, Niyazi Bulut, Omer Kaygili, **A Theoretical Study on Acetophenone Molecule**, Oral Presentation, Anadolu Kongreleri 3. Uluslararası Uygulamalı Bilimler Kongresi, pp. 399-400, 28-29 December 2019, Diyarbakır, Turkey. http://lnnk.in/WEi

PUBLICATIONS:

- Ibrahim Nazem Qader, **Riyadh Saeed Agid**, Srwa Hashim Mohammed, Yousif Hussein Azeez, **Chemical Structural and Vibrational Analysis of Potassium Acetate: A Density Function Theory Study,** Journal of Physical Chemistry and Functional Materials. 2, 1, (2019) 22-24